

BIROn - Birkbeck Institutional Research Online

Gou, L. and Jin, Z. and Pogge von strandmann, Philip and Li, G. and Qu, Y. and Xiao, J. and Deng, L. and Galy, A. (2019) Li isotopes in the middle Yellow River: seasonal variability, sources and fractionation. *Geochimica et Cosmochimica Acta* 248 , pp. 88-108. ISSN 0016-7037.

Downloaded from: <http://eprints.bbk.ac.uk/26027/>

Usage Guidelines:

Please refer to usage guidelines at <http://eprints.bbk.ac.uk/policies.html>
contact lib-eprints@bbk.ac.uk.

or alternatively

Li isotopes in the middle Yellow River: Seasonal variability, sources and fractionation

Long-Fei Gou^{1, 2}, Zhangdong Jin^{1, 3 *}, Philip A. E. Pogge von Strandmann⁴, Gen Li⁵, Yuan-Xin Qu^{1, 2}, Jun Xiao¹, Li Deng¹ & Albert Galy⁶

1. State Key Laboratory of Loess and Quaternary Geology, Institute of Earth Environment, Chinese Academy of Sciences, Xi'an 710061, China;

2. University of Chinese Academy of Sciences, Beijing 100049, China;

3. Institute of Global Environmental Change, Xi'an Jiaotong University, Xi'an 710049, China;

4. London Geochemistry and Isotope Centre (LOGIC), Institute of Earth and Planetary Sciences, University College London and Birkbeck, University of London, Gower Street, London WC1E 6BT, UK;

5. Department of Earth Sciences, University of Southern California, Los Angeles, CA 90089, USA;

6. Centre de Recherches Péetrographiques et Géochemiques, UMR7358, CNRS, Université de Lorraine, 54500 Vandoeuvre les Nancy, France.

*Corresponding author (Zhangdong Jin, zhdjin@ieecas.cn)

Abstract: To evaluate the roles of climate and hydrology in continental-scale silicate weathering, we applied Li isotopes to the Yellow River and systematically investigated seasonal Li flux, Li isotopic compositions and potential sources. We collected samples from the middle reaches of the Yellow River weekly over the full hydrological year of 2013. We find that the dissolved Li is mainly derived from silicates and evaporites in the arid to semi-arid Yellow

27 River basin. Silicate weathering of loess during the monsoonal season
28 dominates the Li flux in the middle reaches of the Yellow River, with a positive
29 relationship between dissolved Li flux and physical erosion rate. Evaporite
30 contribution for riverine Li was relatively constant in the middle reaches of the
31 Yellow River but slightly increased after the storm event, with an average
32 proportion of ~25%, which might represent the proportion of evaporite
33 contribution to global oceans. Seasonal variations in the riverine Li isotopic
34 compositions are dominantly controlled by temperature with a fractionation
35 gradient as -0.182‰ per °C over the full year with deviations likely driven by
36 re-dissolution of suspended **particulate** matter, extreme hydrological events,
37 and groundwater **contribution**. **Temperature dependent $\delta^7\text{Li}$ value variation of**
38 **river water inputted into oceans indicates that Cenozoic climate cooling itself**
39 **may be able to explain ~2‰ of the 9‰ rise of Cenozoic seawater $\delta^7\text{Li}$ value**
40 **(Misra and Forelich, 2012)**. The seasonal variation in riverine Li isotopes
41 highlights that erosion and weathering of loess may provide valuable clues on
42 **secular chemical** weathering and seawater $\delta^7\text{Li}$ variation spanning a range of
43 time scales.

44 **Key words:** Li isotopes, temperature dependency, seasonal variation, loess
45 weathering, the Yellow River, the Chinese Loess Plateau

46 **1. Introduction**

47 Chemical weathering is among the most important geochemical
48 processes operating on Earth's surface, driving the cycling of elements from

49 continents to sedimentary basins and consequently modulating the
50 compositions of the crust (e.g. [Lee, 2008](#); [Teng et al., 2010](#); [Liu and Rudnick,](#)
51 [2011](#); [Liu et al., 2013](#)). Most importantly, chemical weathering of silicate rocks,
52 i.e. silicate weathering, represents a major sink to atmospheric CO₂ over
53 geological timescales, regulating the geological carbon cycle and the
54 long-term evolution of the climate system (e.g. [Walker et al., 1981](#); [Berner et](#)
55 [al., 1983](#); [Gaillardet et al., 1999](#); [West et al., 2005](#)). The rate and intensity of
56 silicate weathering require accurate and precise quantification in order to
57 evaluate the efficiency of neutralizing capacity of CO₂ by silicate weathering.

58 In the past decades, a number of isotopic proxies have been suggested
59 for evaluating weathering rate and intensity, such as Sr, Mg, Si, and Os
60 isotopes. However, none of them would be able to **directly** trace silicate
61 weathering reliably owing to the effects of other processes and/or influences
62 from unconstrained sources, such as biological processes for Mg and Si
63 isotopes ([Li et al., 2014](#); [Mavromatis et al., 2016](#); [Pogge von Strandmann et al.,](#)
64 [2016](#)), meta-carbonates-sourced radiogenic Sr ([Edmond 1992](#); [Galy et al.,](#)
65 [1999](#)), and black shale-derived Os ([Ravizza and Esser, 1993](#)).

66 Due to its low concentration in carbonates and its large mass difference
67 between ⁶Li and ⁷Li, Li isotopes are considered as the most promising tracer of
68 silicate weathering processes currently available ([Chan et al., 1992](#); [Huh et al.,](#)
69 [1998, 2001](#); [Pistiner and Henderson, 2003](#); [Kısakürek et al., 2005](#); [Hathorne](#)

70 and James, 2006; Pogge von Strandmann et al., 2006, 2010, 2013, 2016,
71 2017; Vigier et al., 2008, 2009; Lemarchand et al., 2010; Millot et al., 2010b, c;
72 Misra and Froelich, 2012; Tipper et al., 2012; Bouchez et al., 2013; Dellinger et
73 al., 2014, 2015, 2017; Wanner et al., 2014; Clergue et al., 2015; Vigier and
74 Godd ris, 2015; Wang et al., 2015; Henchiri et al., 2016). Dissolution
75 experiments have proved that negligible Li isotope fractionation occurs during
76 mineral dissolution (Pistiner and Henderson, 2003; Wimpenny et al., 2010,
77 2015; Verney-Carron et al., 2011; Ryu et al., 2014). Significant Li isotopic
78 fractionation is observed when Li is incorporated into the lattices of secondary
79 minerals and/or during adsorption onto the secondary mineral surface (Huh et
80 al., 2001; Vigier et al., 2008; Millot et al., 2010b; Pogge von Strandmann et al.,
81 2010; Wimpenny et al., 2015). Li isotopes have been suggested to trace both
82 silicate weathering intensity (Huh et al., 1998, 2001; Kısak rek et al., 2005;
83 Pogge von Strandmann et al., 2006, 2008a, b, 2010, 2012, 2013, 2016; Millot
84 et al., 2010c; Dellinger et al., 2015, 2017; Wang et al., 2015) and silicate
85 weathering fluxes (Vigier et al., 2009), despite some recent studies showing no
86 universal global correlation between $\delta^7\text{Li}$ and silicate weathering rates (e.g.
87 Pogge von Strandmann et al., 2017).

88 Previous studies have mainly focused on the spatial variation of the
89 riverine dissolved Li isotopes and have explored (1) which factors and what
90 processes control riverine Li isotopic fractionation and (2) how to use Li
91 isotopes as a tracer of silicate weathering at various scales (e.g. Huh et al.,

92 1998, 2001; Pogge von Strandmann et al., 2006, 2008a, b, 2010, 2012, 2013,
93 2016, 2017; Vigier et al., 2008, 2009; Millot et al., 2010b, c; Liu and Rudnick,
94 2011; Liu et al., 2011, 2015; Dellinger et al., 2014, 2015, 2017; Wang et al.,
95 2015). However, the dominant processes controlling riverine Li isotopic ratios
96 remains debatable since fractionation related to physicochemical would
97 involve processes during the riverine transport and/or conservative mixing
98 between isotopically different endmembers. In particular, emphasized
99 processes and sources may affect Li isotopic ratios including:

100 1. The ratio of primary mineral dissolution relative to secondary mineral
101 neoformation or expressed as the proportion of Li adsorption onto and/or
102 incorporated into secondary minerals during weathering and related
103 processes (Huh et al., 2001; Pogge von Strandmann et al., 2006, 2008a, b,
104 2010, 2013, 2016, 2017; Dellinger et al., 2015; Vigier et al., 2008; Millot et
105 al., 2010b; Pogge von Strandmann and Henderson, 2015; Wang et al.,
106 2015; Wimpenny et al., 2015). Specifically, this may be controlled by the
107 subsurface residence time or the water/rock interaction time (Wanner et al.,
108 2014; Liu et al., 2015);

109 2. The presence of evaporites (Huh et al., 1998; Liu et al., 2011; Wang et al.,
110 2015);

111 3. Fractionation factors of Li isotopes may be mineral specific (Wang et al.,
112 2015; Pogge von Strandmann et al., 2017).

113 Kısakürek et al. (2005) and Liu et al. (2015) found that at the same site

114 there was a ~10‰ difference of Li isotopic compositions in different seasons.
115 Some studies explored $\delta^7\text{Li}$ signatures through collecting time-series samples
116 at regional and catchment scales and showed differing, location-specific,
117 seasonal variations of $\delta^7\text{Li}$ (Kisakúrek et al., 2005; Liu et al., 2015; Henchiri et
118 al., 2016; Pogge von Strandmann et al., 2016). However, most time-series
119 data do not have high-enough resolution to decipher the role of climate and
120 extreme hydrological events (e.g. storms) in Li isotopic fractionation, and to
121 eliminate the associated uncertainties. Therefore, further studies with samples
122 collected at higher temporal resolution are required to better understand the
123 responses of $\delta^7\text{Li}$ to changes in climatic and hydrological conditions.

124 In this study, in order to elucidate the significance and utility of riverine Li
125 isotopic fractionation in the context of conservative mixing and related
126 weathering processes, we conducted a comprehensive investigation on (1)
127 how riverine $\delta^7\text{Li}$ is affected by water sources and weathering processes in
128 semi-arid regions; and (2) how and why weathering processes vary over a
129 hydrological year. We collected river water samples under high temporal
130 resolution (weekly) from the middle reaches of the Yellow River, one of the
131 most turbid rivers in the world draining the highly erodible Chinese Loess
132 Plateau (CLP). Owing to seasonal contrast caused by the East Asian summer
133 monsoon, the middle reaches of the Yellow River provide a suitable setting to
134 evaluate the response of riverine Li isotopes to changes in climatic and
135 hydrological conditions.

136

137 **2 Study areas**

138 **2.1 Geography**

139 The Yellow River is the fifth longest river (~5,464 km) in the world, also is
140 known as the most sediment-laden river with 10.8×10^8 t/yr of sediment
141 discharge (Q_s) (Zhang et al., 1995). Originating from the northeastern part of
142 the Qinghai-Tibetan Plateau with an elevation of about 5,000 m, the Yellow
143 River travels across the CLP and enters the Bohai Sea (Zhang et al., 1995; Wu
144 et al., 2008). The upper reaches extend over a length of 3,471 km from the
145 river source to Toudaoguai draining a catchment area of 385,996 km². The
146 middle reaches stretch 1,206 km from Toudaoguai to Huayuankou draining an
147 area of 343,751 km² with dozens of tributaries joining the main stream from the
148 CLP. The lower reaches extend over a length of 786 km from Huayuankou
149 through the flat alluvial plains to the estuary draining an area of 22,726 km²
150 (Wang et al., 2007). Our study area is in the middle reaches of the Yellow River
151 between Toudaoguai to Tongguan that drain the CLP (Fig. 1), characterized by
152 highest annual Q_s along the river (Saito et al., 2001; Chen et al., 2006; Sui et
153 al., 2014).

154 **Though today's erosion rate of the Yellow River is significantly lower (c. 10%**
155 **to what it used to be 50 to 100 years ago, Wang et al., 2007),** because of the
156 high erodibility of loess, the CLP is the largest sediment source to the Yellow
157 River. With 21 tributaries and a total catchment area larger than 1,000 km², the

158 middle reaches of the Yellow River draining the CLP contributes nearly 90% of
159 the total Q_s (Saito et al., 2001; Wang et al., 2010; Yu et al., 2013), though only
160 about 40% of the total water discharge (Q_w) (Jiao et al., 2014; Zhao et al.,
161 2014). By contrast, the upper reaches contribute ~60% of the annual Q_w but
162 merely 10% of the total Q_s and 38%-47% of overall total dissolved solids (TDS,
163 Li et al., 2018) carried by the Yellow River. Both suspended particulate matter
164 (SPM) and TDS are sourced from rapid loess erosion into waters in the middle
165 reaches of the Yellow River dominantly.

166 **2.2 Geology**

167 The Yellow River basin is developed on the old Sino-Korean Shield during
168 the Archeozoic to Proterozoic Eras (Zhang et al., 1995). It displays complex
169 features in lithology and topography, with outcrops including rocks aging from
170 Precambrian to Quaternary. In the upper reaches above Lanzhou (elevation
171 2,000-4,000 m), the bedrock is mainly composed of limestone, low-grade
172 metamorphic rocks and clastic rocks interlaced with volcanic rocks and
173 evaporites (Chen et al., 2005). The middle reaches draining the CLP are
174 mainly covered by Neogene and Quaternary eolian loess and loess-like
175 deposits, accounting for 44% of the total catchment area. Loess is deemed to
176 be relatively homogeneous, porous, friable, pale yellow, typically non-stratified
177 and often calcareous (Liu, 1988), which can represent the average chemical
178 compositions of the upper continental crust (UCC, Taylor et al., 1983), and has
179 a relatively homogeneous Li isotopic composition of $0 \pm 4\text{‰}$ (Teng et al., 2004;

180 [Sauzeat et al., 2015](#)). Mineralogically, loess is composed of quartz, feldspar,
181 calcite, micas, and heavy minerals in minor proportion, with additional minor
182 evaporites, such as halite, gypsum and mirabilite ([Li et al., 1984](#); [Liu, 1988](#);
183 [Zhang et al., 1995](#); [Yokoo et al., 2004](#)), though proportions of these minerals in
184 loess and paleosol layers vary slightly ([Liu, 1988](#)). The erosion operating on
185 the CLP shapes the numerous gullies and rolling topography and sustains the
186 extremely high Q_s of the Yellow River, particularly during the monsoon season.
187 As an erosional product, SPM in the Yellow River is of the same mineralogical
188 and geochemical compositions as loess ([Li et al., 1984](#); [Zhang et al., 1995](#)).

189 **2.3 Climate**

190 The Yellow River basin is characterized by temperate climate. The upper
191 reaches are in the region of cold-arid to semi-arid climate with mean annual
192 temperature ranging from 1°C to 8°C, whereas the middle reaches are
193 semi-arid to semi-humid with mean annual temperature ranging from 8°C to
194 14°C (both records from 1950s-2000s, [Chen et al., 2005](#)). Mean annual
195 precipitation shows significant spatial variations across the river basin,
196 increasing from 368 mm/yr in the upper reaches to 530 mm/yr in the middle
197 reaches ([Wang et al., 2007](#)). Controlled by the East Asian summer monsoon,
198 the seasonal climatic variations are more pronounced than spatial variations.
199 In general, the climate in the Yellow River basin is featured to be cold and dry
200 with less precipitation in winters but warm and wet following rainstorms in
201 summers, especially in the middle reaches. The wet season is from June to

202 mid-September, accounting for 80% of the total annual precipitation (500-600
203 mm/yr, [Zhang et al., 1995](#)).

204

205 **3 Sampling and Methodology**

206 **3.1 Sampling protocol**

207 A total of 60 river water and SPM samples were collected weekly in 2013
208 at the Longmen hydrological station (35°40'06.43"N; 110°35'22.88"E).
209 Hereinto, four samples (Nos. LM13-31 to 34) were collected daily during a
210 storm event that resulted in a maximum Q_w (2400.53 m³/s) in 2013 ([Zhang et](#)
211 [al., 2015](#); [Lei et al., 2016](#)). The Longmen station is located in the middle
212 reaches of the Yellow River, where the tributaries mostly draining the CLP
213 have joined the main stream but excluded both drainages of the Fen and Wei
214 Rivers that drain highly populated areas (Fig. 1). Therefore, anthropogenic
215 impact is minimized whereas weathering and erosion of the CLP is maximized
216 on the station. To constrain atmospheric inputs, three rain water samples were
217 collected in July and August of 2013 at the station with a volume of 60 mL (see
218 below), which is too little to obtain Li isotopic ratios. Thus, a 2 L rain water
219 sample was collected in the summer of 2017 near the station. To estimate
220 contributions from evaporites, five typical loess samples **from different loess**
221 **layers** in Lingtai loess profile were collected for extracting evaporite-sourced Li
222 (see section 3.3.3 below). In addition, one sample of river bed sand (RBS) was
223 also collected right at the center river bed of the Longmen station.

224 All river water samples were collected 0.5 m below the surface in the
225 central part of the river. For each sample, water temperature, pH, electrical
226 conductivity (EC), and TDS were measured. All water samples were filtered
227 on-site using a manual peristaltic pump using 0.2 μm nylon filters. Filtered
228 water samples were stored in pre-cleaned polyethylene bottles. Filters were
229 removed using a pre-cleaned plastic tweezers and placed into glass petri
230 dishes on site in order to obtain SPM. For major cations, Li and Li isotope
231 analyses, 60 mL of water were collected, acidified using ~ 0.25 mL of 6 M
232 distilled HNO_3 to $\text{pH} < 2$ and stored at 4°C at the hydrological station before
233 transportation to the laboratory. A separate pre-cleaned bottle was used for
234 storing unacidified sample for anion analysis. Rainwater samples were treated
235 in the same manner (see [Zhang et al. \(2015\)](#) for details). In order to
236 characterize anthropogenic contribution, an agricultural sewage water sample
237 (TKT1) was collected in the middle reaches of the Yellow River and was also
238 pretreated at the same way.

239 **3.2. Major cations and Li concentration analyses of water samples**

240 Major cations were analyzed by a Leeman Labs Profile inductively
241 coupled plasma atomic emission spectroscopy (ICP-AES), with the RSD
242 (relative standard deviation) better than 1%. Major anions (F , Cl , and SO_4)
243 were analyzed by ion chromatography (ICS 1200) and NO_3 was measured by
244 a Skalar continuous flow analyzer. The RSDs were 2.0% and 2.2%,
245 respectively. Alkalinity (expressed as HCO_3) was measured by Shimadzu

246 Corporation total organic carbon analyzer (TOC-V_{CPH}) with the RSD less than
247 1.5% at Northwest Agriculture and Forestry University (Zhang et al., 2015).

248 Li concentrations of river water samples were conducted at the State Key
249 Laboratory of Loess and Quaternary Geology (SKLLQG) using a PerkinElmer
250 NexION 300D ICP-MS, with the RSD better than 5%.

251 **3.3 Lithium isotopes analyses**

252 Pretreatment and analyses of Li isotopic compositions of all samples were
253 performed at the clean room (class 100) in the SKLLQG, IEE-CAS.

254 **3.3.1 Pretreatment of river water samples**

255 10–20 mL river water and 600 mL rainwater, containing approximately 300
256 ng Li, were evaporated and then treated with a mixture of distilled HNO₃ : HF =
257 1:3 to digest organic matter. The final dried sample was picked up in 2 mL 0.5
258 M HNO₃ for column separation. The agricultural sewage water sample (TKT1)
259 was also pretreated with the same way.

260 **3.3.2 Dissolution of SPM and RBS**

261 SPM samples were washed off the filter with Milli-Q water and evaporated.
262 The dried samples were weighed and then grounded using a pre-cleaned
263 agate mortar. The RBS sample was also treated with the same way. Fractions
264 containing ~300 ng Li were then dissolved using a 1:3 mixture of concentrated
265 HNO₃ and HF, followed by 4 mL aqua regia, and then 4 mL concentrated HNO₃.
266 The final dried sample was dissolved in 2 mL 0.5 M HNO₃ for column
267 separation (Gou et al., 2017).

268 **3.3.3 Experiment of extracting evaporite-sourced Li in loess**

269 Five typical fresh loess samples were used to extract evaporites in loess,
270 following the method described in [Yokoo et al. \(2004\)](#) modified from [Tessier et](#)
271 [al. \(1979\)](#). Briefly, 5 g milled loess were leached by milli-Q water for 5 minutes
272 and then centrifuged following filtration. This leach is aimed at evaporite-
273 sourced ions because of the fast dissolution kinetic of evaporite minerals
274 ([Yokoo et al., 2004](#)). Extracted ions concentration of supernatants were
275 determined using a PerkinElmer NexION 300D ICP-MS and dried then picked
276 up in 2 mL 0.5 M HNO₃ for column separation.

277 **3.3.4 Purification and analysis for Li isotopes**

278 All of the solute samples were purified by single-step cation exchange
279 chromatography filled up with 8 mL resin (Bio-rad® AG50W X-12, 100-200
280 mesh) using a method ([Gou et al., 2017](#)) modified from [James and Palmer](#)
281 ([2000](#)) and [van Hoecke et al. \(2015\)](#), with 0.5 M diluted HNO₃ as an eluent.
282 The purified Li fraction was picked up in 2% HNO₃ and was targeted to be 100
283 µg/L of Li for Multi-Collector Inductively Coupled Plasma Mass Spectrometer
284 (MC-ICP-MS, Neptune plus) measurement. Splits collected before and after
285 the main Li elution peak were assessed for Na and Li contents, to ensure full
286 column recovery. The weight Na/Li ratio in all samples reported in this study
287 was less than 1, which we found to have insignificant effect on the Li isotopic
288 ratio measurements ([Gou et al., 2017, 2018](#)). The total procedural blank of this
289 method was less than 0.16 ng Li, which is insignificant relative to the 300 ng of

290 Li analyzed in each sample ([Gou et al., 2017, 2018](#)).

291 For each sample, triple measurements were performed to obtain the
292 average values as well as standard derivations (s.d.). Two in-house standards
293 were run repeatedly for a one-year period yielding $\delta^7\text{Li}$ as $8.3 \pm 0.2\text{‰}$ (2 s.d., n
294 = 43) for IEECAS-Li, and as $12.2 \pm 0.2\text{‰}$ (2 s.d., n = 59) for SPEX-Li,
295 respectively. In addition, another in-house standard of Isotopic Geochemical
296 laboratory of University of Science and Technology of China (USTC), namely
297 USTC-L, was also run repeatedly at IEE-CAS, yielded a $\delta^7\text{Li} = -19.3 \pm 0.1\text{‰}$ (2
298 s.d., n = 38), in good agreement with that conducted at USTC ($-19.3 \pm 0.2\text{‰}$,
299 [Gou et al., 2017, 2018](#)).

300 Two rock reference materials (AGV-2, BHVO-2) and a seawater reference
301 material (NASS-6) that were purified following the same procedure and
302 measured iteratively to be $\delta^7\text{Li} = 6.7 \pm 0.8\text{‰}$ (2 s.d., n = 13, digestion = 13,
303 column passes = 13), $\delta^7\text{Li} = 3.9 \pm 0.9\text{‰}$ (2 s.d., n = 13, digestion = 13, column
304 passes = 13), and $\delta^7\text{Li} = 31.1 \pm 0.7\text{‰}$ (2 s.d., n = 15, column passes = 15),
305 respectively, over a one year period, all of which are in agreement with
306 previous studies ([Magna et al., 2004](#); [Jeffcoate et al., 2007](#); [Vigier et al., 2009](#);
307 [Pogge von Strandmann et al., 2008a, b, 2010, 2011, 2012, 2013, 2016, 2017](#);
308 [Huang et al., 2010](#); [Lemarchand et al., 2010](#); [Milot et al., 2010a, b](#); [Liu and](#)
309 [Rudnick, 2011](#); [Liu et al., 2013, 2015](#); [Dellinger et al., 2014, 2015, 2017](#); [Pogge](#)
310 [von Strandmann and Henderson, 2015](#); [Wang et al., 2015](#)). Overall, our
311 long-term external reproducibility is better than $\pm 0.9\text{‰}$ (2 s.d.) for $\delta^7\text{Li}$

312 measurements (Gou et al., 2018). Isotopes are all reported relative to the
313 standard L-SVEC (Flesch et al., 1973).

314

315 **4 Results**

316 **4.1 Hydrology and SPM**

317 During the sampling time period, water temperature in the study area
318 increased gradually from January to August and then decreased until the end
319 of the year, ranging from 0°C to 28.8°C, with ice coverage in January and
320 February and peak temperature in August (Fig. 2E). The air temperature near
321 Longmen in 2013 varied similarly to the water temperature. From June to
322 mid-September (monsoon season), the daily air temperature was above 20°C.

323 In the hydrological year of 2013, the total Q_w was 24.53 km³/yr at the
324 Longmen hydrological station (Zhang et al., 2015). The Q_w was constant from
325 January to February, then reached the first peak in March and returned quickly
326 in the middle of April and dropped to an annual minimum period (151.82 m³/s)
327 in May (Fig. 2E). The first Q_w peak from 16th March to 13th April was caused
328 by ice melting when the air temperature was above zero, thus we defined this
329 time period as an “ice melting interval”. During the monsoon season in 2013,
330 the high Q_w reflected the frequent, monsoon-driven rainfall within the Yellow
331 River basin. Notably, a storm event that happens once in a century occurred in
332 the middle reaches of the Yellow River during 22nd and 25th July (Zhang et al.,
333 2015; Lei et al., 2016), resulting in the highest peak Q (2400.53 m³/s) of 2013.

334 After the rainy season, the Q_w declined gradually to a relative low value with
335 some minor fluctuations. The river waters were alkaline over the whole year
336 with pH values ranging between 7.05 and 8.71.

337 SPM in the middle reaches of the Yellow River showed significant
338 seasonal variation, accompanying the Q_w changes (Fig. 2G and H). In contrast
339 to the high concentrations and fluxes of SPM during the monsoon season,
340 SPM was low and constant during the dry seasons with a spike during the ice
341 melting period (Fig. 2G and H). Highest concentrations and fluxes of SPM
342 appeared during the storm event. As a result, physical erosion rate (PER,
343 derived from weekly gauged SPM) during the monsoon season was one to
344 three orders of magnitude higher than that during the dry seasons (Fig. 2I). At
345 the Toudaoguai hydrological station before major tributaries draining the CLP
346 join the Yellow River (Fig. 1), the SPM concentrations are much lower than
347 those of the Longmen station, with limited seasonal variations (Fig. 3). Those
348 observations mean that erosion occurred mainly during the monsoon season,
349 dominated by loess eroded from the CLP into the middle reaches of the Yellow
350 River (Zhang et al., 2015).

351 **4.2 The dissolved Li concentration [Li]**

352 [Li] and $\delta^7\text{Li}$ values of all the time-series river water samples are reported
353 in Figure 2 and Table 1. The dissolved [Li] of our samples from the middle
354 reaches of the Yellow River has an average of 2.80 $\mu\text{mol/L}$, ranging from 2.22
355 $\mu\text{mol/L}$ during the monsoon season to 4.41 $\mu\text{mol/L}$ during the dry season (in

356 winter), with a pronounced seasonal variation as Q_w . Peaks in [Li] are notable
357 during the ice melting and monsoonal intervals. These values are of one order
358 of magnitude higher than those reported in other large rivers (0.22 $\mu\text{mol/L}$ for
359 an average, ranging from 0.05 to 0.8 $\mu\text{mol/L}$; [Huh et al., 1998](#)), but are close to
360 those of the Changjiang (Yangtze) River that also originates from the Tibetan
361 Plateau ([Wang et al., 2015](#)).

362 [Li] of the rain water samples were relatively homogeneous, $\sim 0.13 \mu\text{mol/L}$
363 on average (Table 2), within the range reported by [Millot et al. \(2010a\)](#). Results
364 of water-extraction fraction of the Lingtai loess were reported in Table 3, [Li]
365 varying from 1.5 to 2.0 nmol/g of loess and paleosol samples and 1.3 nmol/g
366 for red clay (RC). As listed in Table 4, RBS [Li] is located within the range of
367 the UCC ([Teng et al., 2004](#); [Sauzeat et al., 2015](#)). Similarly, [Li] in SPM,
368 ranging from 28.9 to 68.9 $\mu\text{g/g}$ (Fig. 2J), is within the range as those in SPM
369 reported elsewhere for rivers draining continental crust (e.g. [Millot et al., 2010c](#);
370 [Dellinger et al., 2015](#); [Liu et al., 2015](#); [Wang et al., 2015](#)). [Li] of the sewage
371 water collected in a farmland near the Longmen hydrological station has a
372 concentration 12.3 $\mu\text{mol/L}$, one order of magnitude higher than the Yellow
373 River water.

374 **4.3 Li isotope compositions**

375 During the sampling period, the dissolved $\delta^7\text{Li}$ values of the river water
376 ($\delta^7\text{Li}_{\text{rw}}$) from the middle reaches of the Yellow River range between 16.9‰ in
377 the summer to 21.5‰ in the winter. This range is smaller than the observed

378 seasonal changes in the Andean and Congo river systems, which were
379 sampled in winter and summer (Liu et al., 2015) or sampled bimestrially
380 (Henchiri et al., 2016), and is much smaller when compared with spatial
381 variations (~40‰, e.g. Vigier et al., 2009; Pogge von Strandmann et al., 2006,
382 2008a, b, 2010, 2012, 2013, 2016, 2017; Millot et al., 2010c; Dellinger et al.,
383 2015; Pogge von Strandmann and Henderson, 2015; Wang et al., 2015).
384 However, our observed range of variation resembles that of the Ganges–
385 Brahmaputra river system with samples from before and after the Indian
386 monsoons (Kisakürek et al., 2005).

387 Clearly seasonal variation was observed for the $\delta^7\text{Li}_{\text{rw}}$ of the middle
388 reaches of the Yellow River. Similarly to [Li] behavior, $\delta^7\text{Li}_{\text{rw}}$ peaked during the
389 ice melting interval. During the monsoon, $\delta^7\text{Li}_{\text{rw}}$ generally increased throughout,
390 with another peak during the storm event (Fig. 2C).

391 The $\delta^7\text{Li}$ values of SPM ($\delta^7\text{Li}_{\text{SPM}}$) were less variable over the sampling
392 year (Fig. 2D), ranging from 0.6‰ to 3.5‰ with an average of $1.8 \pm 0.9\text{‰}$
393 (Table 1). All $\delta^7\text{Li}_{\text{SPM}}$ were much lower than all of $\delta^7\text{Li}_{\text{rw}}$, but within the $\delta^7\text{Li}$
394 ranges of the CLP loess and the UCC (Teng et al., 2004; Tsai et al., 2014;
395 Sauzeat et al., 2015).

396 The rain water (R1YR) has a $\delta^7\text{Li}_{\text{atmo}} = 9.3 \pm 0.1\text{‰}$ (2 s.d., Table 3). This is
397 different with respect to the rain data from elsewhere (e.g. 31‰ in Iceland by
398 Pogge von Strandmann et al. (2006), 33‰ in the Azores by Pogge von
399 Strandmann et al. (2010), and 16‰ in France and 26‰ in Canada by Millot et

400 al. (2010a, c)), suggesting that $\delta^7\text{Li}_{\text{atmo}}$ is strongly dependent on locations.

401 The $\delta^7\text{Li}$ values of the evaporite-sourced Li ($\delta^7\text{Li}_{\text{evap}}$) from loess samples
402 are averaged to be $23.6 \pm 4.8\text{‰}$ (2 s.d., $n = 4$), significantly higher than those
403 of river water and SPM samples (Table 3).

404 The Li isotopic compositions are 6.9‰ for the RBS sample and 23.8‰ for
405 the sewage water respectively, with the latter being higher than all the $\delta^7\text{Li}_{\text{rw}}$
406 (Table 4).

407

408 **5 Discussions**

409 **5.1 Partitioning between dissolved and particulate Li**

410 Fluvial export of Li from continents to basins/oceans has two major forms:

411 1) dissolved in river water and 2) incorporated in particulates as the SPM form.

412 At the global scale, Li is transported mainly as the form of SPM (Misra and

413 Froelich, 2012; Li and West, 2014; Dellinger et al., 2015). To determine how Li

414 partitions between the two forms for the Yellow River, we calculated the

415 proportions of Li transported in the dissolved load (Li_{rw} in %) and SPM (Li_{SPM}

416 in %) using the following equations, following Bouchez et al. (2013) and

417 Gaillardet et al. (2014):

$$418 \quad \text{Li}_{\text{rw}} (\%) = \frac{\text{Li}_{\text{rw}} \text{ flux}}{\text{Li}_{\text{rw}} \text{ flux} + \text{Li}_{\text{SPM}} \text{ flux}} \times 100 \quad \text{Eq. (1)}$$

$$419 \quad \text{Li}_{\text{SPM}} (\%) = 100\% - \text{Li}_{\text{rw}} \quad \text{Eq. (2)}$$

420 where the Li_{rw} and Li_{SPM} fluxes are in t/yr of dissolved and SPM loads (Fig. 2A

421 and G), respectively. The Li_{rw} flux is the product of $[\text{Li}]$ of river water and the

422 corresponding one-week average Q_w gauged (generally, three times/day) in
423 the sampling site. Similarly, the Li_{SPM} flux is calculated by multiplying [Li] of
424 SPM and the corresponding one-week average SPM concentration gauged as
425 same as Q_w in the sampling site. The results show that 73.3%-98.5% of the
426 total exported Li was transported as SPM form in the middle Yellow River in
427 2013, in excellent agreement with its dominated particulate form in global
428 rivers as suggested by previous studies. Note that this calculation does not
429 consider the potential variability of the Li content of SPM with water depth. For
430 example, [Dellinger et al. \(2014, 2015\)](#) reported heterogeneous SPM [Li] and
431 [δ^7Li_{SPM}] along vertical sections in the Amazon because of the dilution by
432 increasing quartz proportions along vertical profile in rivers, although [Pogge
433 von Strandmann et al. \(2017\)](#) reported a homogeneous SPM [δ^7Li_{SPM}] from
434 surface to bottom in the Ganges. A similar [Li] of the RBS sample (36.8 $\mu g/g$) to
435 those of the SPM as well as loess ([Li et al., 1984](#)) may indicate a
436 homogeneous [Li] of SPM with water depth in the middle reaches of the Yellow
437 River, and if this is the case, our estimated Li_{SPM} flux likely represents a
438 reasonable estimation of the Li_{SPM} flux in the middle reaches of the Yellow
439 River. **Nevertheless, it should be beard in mind that the depth-profile variability
440 of SPM content as well as sediment chemistry may shed some uncertainty on
441 this estimation.**

442 More than 60% of the annual dissolved Li transported by the Yellow River
443 waters occurs during the monsoon season, due to the high Q_w (Fig. 2A).

444 During the dry seasons when SPM fluxes are low (dozens mg/L), Li_{rw} flux is
445 relatively constant compared to Li_{SPM} , with two peaks during the ice melting
446 period and in the early January (Fig. 2A). The highest proportion (26.7%) of
447 Li_{rw} relative to Li_{SPM} is observed in the early January for the sampling year
448 when the Yellow River was frozen.

449 **5.2 Sources of dissolved Li**

450 Previous studies have suggested that dissolved Li is predominated by
451 silicate weathering, so that carbonate weathering is negligible regardless of
452 the covering proportions of carbonates within river basins (Kısakürek et al.,
453 2005; Millot et al., 2010c; Dellinger et al., 2015; Wang et al., 2015), which is a
454 premise to use Li isotopes tracing silicate weathering (e.g. Huh et al., 1998,
455 2001; Kısakürek et al., 2005; Vigier et al., 2009; Millot et al., 2010c; Dellinger
456 et al., 2015; Wang et al., 2015). However, recent work revealed that in the
457 Changjiang River evaporites likely contribute nearly half of the dissolved Li in
458 river waters because of the wide-spread evaporites in its head watersheds and
459 their fast dissolution kinetics (Liu et al., 2011; Wang et al., 2015). Likewise,
460 although loess is lithologically homogeneous and represents the composition
461 of the UCC, there is about 5-10% of evaporites in loess (Zhang et al., 1995),
462 which contribute solutes significantly to the Yellow River waters (Zhang et al.,
463 2015).

464 The evaporites in the loess of the CLP are dominated by halite, gypsum,
465 and mirabilite (Zhang et al., 1990; Yokoo et al., 2004). Because of their faster

466 dissolution kinetics, dissolution of evaporites readily contributes Na, Cl, B, SO₄,
467 and Li to the rivers (Zhang et al., 2015). The observed positive correlations
468 between [Li] and [B], [Cl], [Na], and [SO₄] of river waters (Fig. 4) indicate that
469 there is substantial contribution from evaporites to the dissolved Li in the
470 Yellow River (Fig. 5), given the fact that calculated rain contribution is limited
471 (see the following section 5.2.1). The deviation during the early monsoon
472 (purple shadow in Fig. 5) may be attributed to the input of groundwater when
473 rains have been penetrating, as indicated by the major ions (Zhang et al.,
474 2015), resulting from slightly increase in contribution from silicates. Thus, it is
475 important to discern the parts of Li from sources other than silicates.

476 **5.2.1 Atmospheric input**

477 To correct the dissolved [Li] from input of atmosphere, we refer to the three
478 rain water samples collected at the Longmen station during the rainy season.
479 These three rain water samples yield an average Li/Cl molar ratio of $1.18 \pm$
480 0.96×10^{-3} . Given that the evapotranspiration correction factor (F) is 1.76
481 (1.61-1.90, Zhang et al., 2015) at the CLP area, we estimated the Li in river
482 waters derived from atmosphere ($[Li]_{atmo}$) to be $0.22 \pm 0.28 \mu\text{mol/L}$, which
483 accounts 5%-10% of Li in river waters from the middle reaches of the Yellow
484 River (Fig. 6). This contribution is in the same range as in the Changjiang but is
485 much higher than that of the Amazon River (~2%, Dellinger et al., 2015). **The**
486 **high contribution of atmospheric input for the Yellow River is likely caused by**
487 **high dust activities from inland Asia** (Jin et al., 2011).

488 5.2.2 Anthropogenic inputs

489 Within the upper and middle reaches of the Yellow River basin, the
490 anthropogenic activities are dominated by agriculture (grazing, farming, etc.
491 [Chen et al., 2003](#)) with limited industry. However, it is difficult to quantify
492 agriculture input due to the highly spatiotemporal variations of Li contributions
493 and its isotopic compositions of fertilizers; this estimation can be precarious
494 unless sewage has a stable chemical composition, which is extremely unlikely
495 ([Chetelat et al., 2008](#)). Herein, because of the relatively higher NO_3^- than that
496 of the natural river waters, we assumed that all NO_3^- is from fertilizers ([Chen et](#)
497 [al., 2003](#); [Zhang et al., 2015](#); [Fan et al., 2016](#)). Then, using the typical fertilizer
498 compositions, (i.e. $\text{NO}_3^-/\text{Na} = 7 \pm 3$, $\text{Cl}/\text{Na} = 4 \pm 1$, and $\text{SO}_4/\text{Na} = \sim 1$, [Roy et al.,](#)
499 [1999](#); [Chetelat et al., 2008](#)), and Li/Na ratio (1.36×10^{-5}) and Li isotopic
500 composition ($23.8 \pm 0.2\text{‰}$, defined as $\delta^7\text{Li}_{\text{anth}}$) of the sewage water we
501 collected in a farmland in the middle Yellow River (Table 4) as end-member of
502 anthropogenic inputs ($[\text{Li}]_{\text{anth}}$), Li input by anthropogenic activity can be
503 approximately quantified. Our first-order estimates show that the $[\text{Li}]_{\text{anth}}$ to the
504 middle reaches of the Yellow River range from 0.4% to 1.6%. These inputs are
505 quite limited compared to that of the Changjiang River ([Chetelat et al., 2008](#);
506 [Wang et al., 2015](#)), and this may be due to the fact that the Changjiang River
507 drains across the highly developed industrial areas in central and southeastern
508 China.

509 The limited $[\text{Li}]_{\text{anth}}$ is also supported by lower $\delta^7\text{Li}_{\text{rw}}$ in the middle reaches

510 of the Yellow River in summer. Since agriculture activities generally occur in
511 summer (Chen et al., 2003) and fertilizers are well known to have abnormally
512 high $\delta^7\text{Li}$ (Qi et al., 1997; Kısakürek et al., 2005; Millot et al., 2010b; Négrel et
513 al., 2010), $\delta^7\text{Li}_{\text{rw}}$ in summer would be quite high if $[\text{Li}]_{\text{anth}}$ was significant.

514 **5.2.3. Carbonate weathering**

515 Previous studies have revealed that Li in river waters is scarcely derived
516 from carbonates (Kısakürek et al., 2005; Millot et al., 2010c; Dellinger et al.,
517 2015; Wang et al., 2015). Here, by assuming that all Ca in waters in the middle
518 reaches of the Yellow River is from carbonate dissolution and using a typical
519 carbonate Li/Ca molar ratio of $1.5 \pm 0.5 \times 10^{-5}$ (Hathorne and James, 2006;
520 Hathorne et al., 2009; Pogge von Strandmann et al., 2013), we calculated the
521 Li derived from carbonates ($[\text{Li}]_{\text{carb}}$). The results showed that $[\text{Li}]_{\text{carb}}$ to the
522 middle reaches of the Yellow River is ~4.1% on average, ranging from 0.4% to
523 7.4%. This is the upper limit of $[\text{Li}]_{\text{carb}}$, since silicate dissolution also brings Ca
524 to river water (Zhang et al., 2015; Li et al., 2018), with a silicate Ca/Na = 0.2 ~
525 0.5, such as in the upper Yellow River (Wu et al., 2005). It is thus reasonable
526 to conclude that carbonates contribution to Li in river waters in the middle
527 reaches of the Yellow River is very small (Fig. 6), similar to most of large rivers
528 in the world (Huh et al., 1998; Millot et al., 2010c; Bagard et al., 2015; Dellinger
529 et al., 2015; Henchiri et al., 2016; Wang et al., 2015; Pogge von Strandmann et
530 al., 2017). For such a low $[\text{Li}]_{\text{carb}}$, the carbonate effect on $\delta^7\text{Li}_{\text{rw}}$ is likely to be
531 negligible.

532 **5.2.4 Evaporite dissolution**

533 As mentioned above, evaporite dissolution may contribute to riverine Li
534 significantly in the Yellow River waters (Zhang et al., 2015), because of 1)
535 rapid dissolution kinetics of evaporites, 2) high dissolved [Cl] in river waters
536 over the full sampling period, and 3) linear relations between [Li] and [Cl], [Na],
537 [SO₄] and [B] (Fig. 4). However, evaporite contribution to major ions in the
538 upper reaches of the Yellow River is quite limited (i.e. from 12.4% to 15.9%, Li
539 et al., 2018), compared to that of its middle reaches (28.4% to 66.3%, Zhang et
540 al., 2015), indicating that riverine Li from evaporites in the Yellow River ([Li]_{evap})
541 is also mainly sourced from the CLP as SPM.

542 Based upon loess-extraction experiments, the evaporites in loess have
543 $\text{Li}/\text{Na}_{\text{evap}} = 2.52 \pm 1.39 \times 10^{-4}$ and $\delta^7\text{Li}_{\text{evap}} = 23.6 \pm 4.8\text{‰}$ (2 s.d., n = 4),
544 respectively (Table. 3). Using this $\text{Li}/\text{Na}_{\text{evap}}$ ratio and the part of Na in river
545 waters from evaporites ($[\text{Na}]_{\text{evap}}$, Zhang et al., 2015), we estimated $[\text{Li}]_{\text{evap}}$ by
546 the following equation:

$$547 \quad [\text{Li}]_{\text{evap}} = [\text{Na}]_{\text{evap}} \times \text{Li}/\text{Na}_{\text{evap}} \quad \text{Eq. (3)}$$

548 The results show that $[\text{Li}]_{\text{evap}}$ ranges from 16.7% to 37.6% (with an average
549 of 25.2%) in the Yellow River water samples (Fig. 6), highlighting the
550 importance of evaporite contribution to the riverine dissolved Li as observed in
551 the Changjiang River (Wang et al., 2015). The contribution of $[\text{Li}]_{\text{evap}}$ to river
552 waters in the middle reaches of the Yellow River also shows seasonal
553 variations in 2013. In early January, $[\text{Li}]_{\text{evap}}$ accounted for ~30% of the riverine

554 Li. After the storm event, $[Li]_{\text{evap}}$ increased dramatically and generally stayed at
555 a high level for the rest of the year, contributing by as much as 37.6% Li to river
556 water. Generally, $[Li]_{\text{evap}}$ was positively correlated with Q_w due to evaporites
557 fast dissolution kinetics. The high Li isotopic ratios of evaporites likely affect
558 the δ^7Li_{rw} , driving it higher when evaporites contribute to a greater part. This is
559 certainly observable immediately after the storm event (Figs. 5 and 7) and
560 further highlights the importance of evaporite dissolution to riverine Li in such
561 arid to semi-arid areas (Zhang et al., 2015). The reason why $[Li]_{\text{evap}}$ did not
562 increase instantaneous following the storm event is that water chemistry
563 generally lags rapid Q_w changes in riverine systems (Godsey et al., 2009;
564 Maher, 2011), and this is likely true in the middle reaches of the Yellow River.
565 To the best of our knowledge, this represents the very first insight into Li
566 isotopic compositions response to an abnormal hydrological event.

567 To date, a few studies have attempted to reveal the evaporite contribution
568 to dissolved Li in river waters, using mixing equations to estimate the
569 proportion of evaporite contribution (Huh et al., 1998; Liu et al., 2011; Wang et
570 al., 2015; Dellinger et al., 2015). Huh et al. (1998) pointed out that evaporites
571 would contribute significant Li to river water, but lacked quantified estimation.
572 Liu et al. (2011) estimated that Li in the upper Changjiang tributaries is
573 exclusively derived from evaporites. Wang et al. (2015) calculated evaporite
574 contribution to Li in river water being from 20% to 55%. In contrast, Dellinger et
575 al. (2015) estimated only <1% Li from evaporites in most tributaries of the

576 Amazon River. Our estimates (averaging 25%) fall within these estimates.
577 Given the representativeness of loess to chemical and Li isotopic compositions
578 of the UCC (Taylor et al., 1983; Teng et al., 2004), this proportion of $[Li]_{\text{evap}}$ in
579 the Yellow river may reflect an average Li contribution of evaporites to global
580 oceans, i.e. ~25%.

581 Overall, our most important observations are: (1) evaporite dissolution
582 brought more Li after the storm event and (2) this higher $[Li]_{\text{evap}}$ was apparently
583 sustained for at least half of one year (Figs. 6 and 7). Despite the wide
584 distribution of evaporites and their fast dissolution kinetics in arid and semi-arid
585 areas (e.g. deserts) rarely accessible to fluids, it is plausible that a large
586 hydrological event promotes their dissolution and then ultimately contributes to
587 river water (Fig. 7).

588 It is important to point out that this Na-normalized calculation for $[Li]_{\text{evap}}$
589 should be considered as an upper limit of evaporite contribution to Li in the
590 Yellow River, because Li would be partially incorporated into secondary
591 minerals (clays and some oxides) due to its high affinity whereas Na is largely
592 conservative in river waters.

593 **5.2.5. Silicate weathering**

594 Apart from the above sources, the rest of Li in river waters is thought to be
595 from silicate weathering ($[Li]_{\text{sil}}$), and this portion is calculated using the
596 following equation (e.g. Wang et al., 2015):

$$597 \quad [Li]_{\text{sil}} = [Li]_{\text{rw}} - [Li]_{\text{atmo}} - [Li]_{\text{anth}} - [Li]_{\text{evap}} - [Li]_{\text{carb}} \quad \text{Eq. (4)}$$

598 Among the five sources for dissolved Li in the middle reaches of the
599 Yellow River as shown in Figure 6, silicate weathering is the dominant source
600 of Li, accounting for ~61.8% on average, ranging from 46.1% to 65.5%. This
601 contribution is close to that observed in the Changjiang River, ranging between
602 45% and 95% (Wang et al., 2015). Hence, silicates and evaporites represent
603 two most important sources of Li to the river waters of the Yellow River.

604 It is noteworthy that even in such scenario for whose water chemistry is
605 dominated by carbonate weathering and evaporite dissolution (Chen et al.,
606 2003; Ran et al., 2015; Zhang et al., 2015; Fan et al., 2016), sources of Li in
607 the Yellow River waters are dominated by silicate weathering (Fig. 6), further
608 supporting the robustness of Li isotopes to be a tracer for silicate weathering
609 (Kisakürek et al., 2005; Dellinger et al., 2015, 2017; Liu et al., 2015).

610 **5.3 Fractionation of riverine Li isotopes ($\delta^7\text{Li}_{\text{rw}}$)**

611 In order to discuss Li fractionation during silicate weathering alone,
612 previous studies attempted to distinguish $\delta^7\text{Li}_{\text{sil}}$ from $\delta^7\text{Li}_{\text{rw}}$ based on mass
613 balance principles (e.g. Wang et al., 2015). In fact, any sourced Li would be
614 fractionated further once they are released into aqueous systems. Since
615 riverine Li in the middle Yellow River is dominated by silicate-sourced, with
616 relative constant $\delta^7\text{Li}_{\text{evap}}$, we discussed the seasonal variation of $\delta^7\text{Li}_{\text{rw}}$ to
617 understand fractionation and silicate weathering processes in the middle
618 Yellow River in the following section.

619 There are two key observations in the middle reaches of the Yellow River.

620 (1) [Li] in SPM range from 28.9 to 68.9 $\mu\text{g/g}$ (Fig. 2J), which lies in the same
621 range of SPMs from the Amazon and the Changjiang Rivers (e.g. [Dellinger et](#)
622 [al., 2014, 2017; Wang et al., 2015](#)), but it is slightly higher than that in loess
623 ([Teng et al., 2004; Tsai et al., 2014; Sauzeat et al., 2015](#)). This could be the
624 result of the inheritance of slightly heterogeneous loess, but also correspond to
625 the uptake into secondary minerals transported as SPM. (2) The constant
626 $\delta^7\text{Li}_{\text{SPM}}$ values ($1.9 \pm 0.9\text{‰}$, 2 s.d.) are much lower than those of river waters
627 ($\sim 15 \pm 5\text{‰}$). Given that Li isotopic fractionation (1) is negligible during
628 dissolution of primary minerals ([Pistiner and Henderson, 2003; Wimpenny et](#)
629 [al., 2010, 2015; Verney-Carron et al., 2011; Ryu et al., 2014](#)) and (2) is neither
630 affected by biological processes ([Lemarchand et al., 2010; Clergue et al., 2015;](#)
631 [Pogge von Strandmann et al., 2016](#)) nor by redox state change ([Faure and](#)
632 [Mensing, 2005](#)), these observations together support an enrichment of ^6Li to
633 SPM, resulting from a preferential scavenging of ^6Li into/onto SPMs from
634 aqueous solutions ([Huh et al., 1998, 2001; Kısakürek et al., 2005; Pogge von](#)
635 [Strandmann et al., 2006, 2008a, b, 2010, 2012, 2013, 2016, 2017; Millot et al.,](#)
636 [2010c; Vigier et al., 2009; Dellinger et al., 2014, 2015, 2017; Wang et al.,](#)
637 [2015](#)). The lack of correlation between the $\delta^7\text{Li}_{\text{rw}}$ and the SPM concentration at
638 Longmen (Fig. 8A) suggests that such preferential scavenging of ^6Li is likely to
639 be occurred within each watershed rather than in main river system. This
640 means (1) that ^6Li scavenging SPM may require more time than the resident
641 time of river water at the ionic strength of the middle reaches of the Yellow

642 River or (2) that Li on loess surface is already saturated when Li reaches the
643 main stream of the river.

644 As mentioned above, the dominant source of Li for both river waters and
645 SPMs in the middle reaches of the Yellow River is loess whose $\delta^7\text{Li}$ signature
646 of silicate phase ($\delta^7\text{Li}_{\text{sil-loess}}$) ranges from 2.5‰ to 4.7‰ (Tsai et al., 2014). The
647 systematically higher $\delta^7\text{Li}_{\text{rw}}$ of waters in the middle reaches of the Yellow River
648 relative to $\delta^7\text{Li}_{\text{sil-loess}}$ reflects the proportion of Li adsorbed into the clay and/or
649 incorporated in the formation of secondary minerals, rather than inherited from
650 the lithology. This can be further depicted by plotting $\delta^7\text{Li}_{\text{rw}}$ and Li/Na molar
651 ratio sourced from silicate weathering ($\text{Li}/\text{Na}_{\text{sil}}$). Both as alkali metals, Li and
652 Na are soluble, but Na is less incorporated into secondary minerals compared
653 to Li, such that $\text{Li}/\text{Na}_{\text{sil}}$ ratio sometimes behaves similarly to $\delta^7\text{Li}_{\text{rw}}$ (Wanner et
654 al., 2014; Dellinger et al., 2015; Liu et al., 2015; Pogge von Strandmann and
655 Henderson, 2015; Wang et al., 2015; Pogge von Strandmann et al., 2016,
656 2017). The low $\text{Li}/\text{Na}_{\text{sil}}$ but high $\delta^7\text{Li}_{\text{rw}}$ likely result from more Li scavenged
657 into/onto SPM during silicate weathering in watersheds, such as during the
658 post-monsoon period. In contrast, $\delta^7\text{Li}_{\text{rw}}$ would become lower if more Li
659 remains in solution (Huh et al., 2001; Wanner et al., 2014; Dellinger et al., 2015;
660 Liu et al., 2015; Pogge von Strandmann and Henderson, 2015; Wang et al.,
661 2015; Pogge von Strandmann et al., 2016, 2017), as those during the late
662 monsoon.

663 Re-dissolution of secondary minerals is suggested to affect $\delta^7\text{Li}_{\text{rw}}$

664 compositions, such as in the lowland Amazon Rivers (Dellinger et al., 2015).
665 Due to freezing and/or ice cover conditions that prevents loess erosion and
666 slows the solid transport during the non-monsoon seasons (Ran et al., 2015;
667 Zhang et al., 2015), the SPM concentrations appeared to be the lowest and
668 Li_{rw} (%) were the highest within the year in the winter season (Fig. 2A).
669 Meanwhile, the low Q_w resulted in a transport-limited weathering scenario in
670 the middle reaches of the Yellow River. As a result, lower δ^7Li_{rw} could be
671 caused by re-dissolution of secondary minerals (Bouchez et al., 2013;
672 Dellinger et al., 2015; Wang et al., 2015) in the middle reaches of the Yellow
673 River during the non-monsoon and our observations support this (Figs. 2B and
674 5).

675 **5.4 Temperature controlled seasonal variations in δ^7Li_{rw} and its global** 676 **implication**

677 In the middle reaches of the Yellow River, the seasonal $[Li]_{sil}$ in 2013 vary
678 from 1.28 to 2.94 $\mu\text{mol/L}$. The magnitude by a factor of two in $[Li]_{sil}$ variation is
679 broadly consistent with the contrasting seasonality of Q_w in the middle reaches
680 of the Yellow River. The East Asian summer monsoon brings sufficient rainfall
681 during the summer, resulting in a dilution of the $[Li]_{sil}$ during the monsoonal
682 season. However, the dilution in $[Li]_{rw}$ and $[Li]_{sil}$ is subdued by comparison to
683 the rise in Q_w , leading to a rise in the Li flux during the monsoon (Figs. 2 and 9).
684 Similar seasonal pattern in alpine environments was also observed elsewhere
685 and related to the Indian monsoon (Galy and France-Lanord, 1999; Tipper et

686 al., 2006). Considering that Li is not involved in terrestrial biological cycles
687 (Lemarchand et al., 2010; Clergue et al., 2015; Pogge von Strandmann et al.,
688 2016) and that vegetation on the CLP is sparse, $[\text{Li}]_{\text{sil}}$ should not be affected by
689 biological processes in the middle reaches of the Yellow River. Rather, $[\text{Li}]_{\text{sil}}$
690 should be dominantly controlled by evaporation/dilution processes at the first
691 order, and then by the balance between silicate weathering and incorporation
692 into secondary minerals. There is a positive power-law relationship between
693 the Li_{sil} flux and PER (Fig. 9), which could support the great importance of
694 physical erosion in dissolved Li fluxes (Gaillardet et al., 1999; Li and West,
695 2014), especially in such loess-dominated rapidly eroding landscapes.
696 However, the relationship indicates that both PER and Li_{sil} are closely linked
697 with Q_w in this weathering-limited region covered by easy erodible loess. Such
698 direct response must be seen as a result of hydrological variations that
699 mobilize different reservoirs characterized by different weathering processes
700 (Calmels et al., 2011). As discussed above, Li isotopes should only equilibrate
701 with the solid before into the main channel rather than during the transportation
702 in the main river, even when SPM is particularly abundant such as in the
703 middle reaches of the Yellow River. Together with the lack of overall
704 relationship between SPM concentration and $\delta^7\text{Li}_{\text{rw}}$ (Fig. 8A), those facts
705 further support the idea that seasonal variation in $\delta^7\text{Li}_{\text{rw}}$ in weathering-limited
706 regimes such as the CLP is a strong kinetic control and temperature sensitivity
707 (West et al., 2005). A negative correlation between river water $\delta^7\text{Li}_{\text{rw}}$ and water

708 temperature over the entire hydrological year was observed, i.e. riverine $\delta^7\text{Li}_{\text{rw}}$
709 decreases with increasing temperature (Fig. 8B).

710 Similar to the kinetic of clay neoformation in soils, such fractionation of
711 riverine Li is likely to represent an isotopic equilibrium that is dominantly
712 dependent on temperature (West et al., 2005). For example, Li and West
713 (2014) suggested a gradient change of $\sim -0.183\text{‰}$ per $^{\circ}\text{C}$ for Li fractionation.
714 For the large range (28.8°C in 2013) of seasonal temperature in this case, the
715 effect would be $>5\text{‰}$ for $\delta^7\text{Li}$, assuming temperature as a single fractionation
716 factor alone, which is exactly the entire observed $\delta^7\text{Li}_{\text{rw}}$ range in the Yellow
717 River. Consequently, the seasonal $\delta^7\text{Li}_{\text{rw}}$ variation in the middle reaches of the
718 Yellow River is likely due to neoformation of Li-bearing secondary
719 aluminosilicates within the watersheds under various temperature conditions.

720 The temperature dependency is described as the following equation:

$$721 \quad 1000 \ln \alpha_{\text{water-clay}} = A(1000000/T^2) + B \quad \text{Eq. (5)}$$

722 where $\alpha_{\text{water-clay}}$ is the fractionation factor between $\delta^7\text{Li}$ in waters and clays in
723 soils; A and B have been empirically determined to be 1.83 and -0.72,
724 respectively (Li and West, 2014). We fit our data by excluding the samples
725 ($\sim 1/8$) that might have experienced SPM re-dissolution (Fig. 5, $[\text{Li}] > 3.15$ in
726 Table 2) and assuming a $\delta^7\text{Li} = 0\text{‰}$ of the water prior to clay formation (Teng
727 et al., 2004). Using Isoplot®, the fitted A and B parameters in Eq. (5) are 1.82
728 ± 0.54 and -2.9 ± 6.5 , respectively, for the observed data (Fig. 8B). The very
729 good agreement for A with literature data further supports our hypothesis.

730 Fitted values for B are imprecise but also encompass literature values. The fit
731 suggests that the Yellow River $\delta^7\text{Li}_{\text{rw}}$ can be perfectly interpreted by
732 temperature-dependent Li fractionation (Fig. 10), although there is a shift of
733 around 2‰ during January and February that might have resulted from SPM
734 re-dissolution as mentioned above (Fig. 5). Indeed, it is important to note that a
735 temperature-dependence has been proposed in several previous studies
736 (Marschall et al., 2007; Li and West 2014) and should exist due to standard
737 isotopic fractionation effects. However, it has never been directly observed in
738 rivers (i.e. Fig. 10), which probably due to the sparse seasonal sample
739 collection (e.g. Kısakürek et al., 2005; Liu et al., 2015; Henchiri et al., 2016;
740 Pogge von Strandmann et al., 2016) and/or limited temperature variation of the
741 reported rivers (e.g. $<14^\circ\text{C}$, Galy and France-Lanord, 1999; Kısakürek et al.,
742 2005; Tipper et al., 2006; Liu et al., 2015; Henchiri et al., 2016). Benefiting
743 from the large temperature discrepancy and relative homogeneous loess, for
744 the first time, we directly observed such temperature dependency of Li isotopic
745 fractionation in river waters (Fig. 10).

746 Given that seasonal $\delta^7\text{Li}_{\text{rw}}$ in the middle reaches of the Yellow River is
747 chiefly controlled by temperature and not by SPM-water interaction, it is worth
748 estimating $\delta^7\text{Li}_{\text{rw}}$ variation regulated by temperature in the world rivers. The
749 previously reported seasonal temperature ranges from 3°C to 14°C in the
750 world rivers (Galy and France-Lanord, 1999; Kısakürek et al., 2005; Tipper et
751 al., 2006; Liu et al., 2015; Henchiri et al., 2016), which is much less than that in

752 the middle reaches of the Yellow River (28.8°C in 2013). Using [Li and West](#)
753 [\(2014\)](#)'s gradient or our fitted one (see Eq. (5) and Fig. 8B), 14°C range could
754 result in about 2‰ $\delta^7\text{Li}$ variation at most. Considering current external
755 precision for Li is around 1‰ (e.g. [Magna et al., 2004](#); [Jeffcoate et al., 2007](#);
756 [Vigier et al., 2009](#); [Pogge von Strandmann et al., 2008a, b, 2010, 2011, 2012,](#)
757 [2013, 2016, 2017](#); [Huang et al., 2010](#); [Lemarchand et al., 2010](#); [Millot et al.,](#)
758 [2010a, b](#); [Liu and Rudnick, 2011](#); [Liu et al., 2013, 2015](#); [Dellinger et al., 2014,](#)
759 [2015, 2017](#); [Pogge von Strandmann and Henderson, 2015](#); [Wang et al., 2015](#);
760 [Gou et al., 2018](#)), it is unlikely to observe such a subtle temperature
761 dependency for Li isotopic fractionation directly in these reported rivers,
762 especially after modifications from other sources and fractionation.

763 Since loess in the CLP represents well the UCC, our temperature
764 dependence of riverine $\delta^7\text{Li}_{\text{rw}}$ variation in the middle reaches of the Yellow
765 River (Fig. 10) indicates that Cenozoic climate cooling itself may be able to
766 only explain ~2‰ of the 9‰ rise of Cenozoic seawater $\delta^7\text{Li}$ assuming that
767 overall Cenozoic temperature decreased c. 15°C ([Zachos et al., 2001](#)),
768 besides increased tectonic uplift and accelerated continental denudation
769 ([Misra and Forelich, 2012](#)). This is an additional temperature-dependent
770 fractionation than that proposed during the Li sink from seawater by [Coogan et](#)
771 [al. \(2017\)](#). Furthermore, a shift to lower seawater $\delta^7\text{Li}$ during the middle
772 Miocene ([Misra and Froelich, 2012](#)) might be a result of an enhanced
773 dissolved Li flux to the oceans owing to an increased silicate weathering driven

774 by an intensified summer monsoon (Clift et al., 2008). In contrast, the more
775 extreme but shorter trends towards lighter Li isotopes reported during
776 hyperthermal Oceanic Anoxic Events (OAEs) (Pogge von Strandmann et al.,
777 2013; Lechler et al., 2015) are far less dominated by temperature changes. For
778 example during the Cenomanian-Turonian OAE2 warming was around 5°C
779 (Forster et al., 2007; Damsté et al., 2010), which would only lead to ~0.75‰ of
780 the 15‰ $\delta^7\text{Li}$ excursions observed (Pogge von Strandmann et al., 2013).

781 **6 Conclusions**

782 This work presents a high-temporal resolution dataset of the riverine
783 dissolved Li flux and Li isotopic compositions and calculates contributions from
784 different sources for river water samples collected weekly from the middle
785 reaches of the Yellow River covering one full hydrological year. The following
786 observations and conclusions were obtained:

787 1. The dissolved load exhibited significant seasonal $\delta^7\text{Li}$ variation in the middle
788 reaches of the Yellow River. The riverine dissolved $\delta^7\text{Li}$ (+16.9‰ to +21.5‰) is
789 fractionated toward higher values compared to the suspended sediments (+1.8
790 \pm 0.9‰) as a result of the temperature-dependent scavenging of ^6Li by
791 secondary minerals within watersheds. SPM re-dissolution, extreme
792 hydrological events, groundwater contribution, and presence of evaporite
793 deviate river water $\delta^7\text{Li}$ to some extent.

794 2. Weathering of silicate minerals from loess dominates the dissolved Li in the
795 middle reaches of the Yellow River. Evaporites contribute ~25% approximately

796 to the total riverine dissolved Li. Because loess represents well the UCC
797 composition, it is plausible that evaporites may contribute ~25% Li to the total
798 Li flux continents to oceans.

799 3. The seasonal variation in the dissolved $\delta^7\text{Li}_{\text{rw}}$ of the middle reaches of
800 the Yellow River can be best interpreted through the temperature dependent Li
801 isotope fractionation at the first order.

802 This study provides novel insights into chemical weathering in the Yellow
803 River basin in the context of monsoonal climates and rapidly eroding CLP, as
804 well as Li dynamics in modern environments. Our observations of the
805 significant Li_{sil} fluxes and unique Li isotopic compositions carried by the Yellow
806 River, in particular the temperature-dependence of Li chemistry, have profound
807 implications for the Cenozoic evolution of seawater Li chemistry and carbon
808 cycle.

809

810 **Acknowledgements:** This work was financially supported by the Key Research Program
811 of the CAS (QYZDJ-SSW-DQC033) and the NSFC Program (41773149). PPvS is
812 supported by ERC Consolidator grant 682760. Mathieu Dellinger and Joshua West are
813 specially thanked for their insightful comment that largely improved this manuscript. We
814 thank He Sun, Fang Huang, Hui-Min Yu, Ying-Zeng Gong and Feng-Tai Tong at University
815 of Science and Technology of China (USTC) for their help and suggestions to the sample
816 preparation and laboratory works, and for their insightful discussions during the
817 manuscript preparation. Special thanks to Jinlong Qiao at the Longmen hydrological

818 station for his assistance with sample collection. We are grateful to two anonymous
819 referees for their constructive comments that greatly improved this manuscript.

820

821 **References:**

822 Bagard M. L., West A. J., Newman K. and Basu A. R. (2015) Lithium isotope fractionation
823 in the Ganges–Brahmaputra floodplain and implications for groundwater impact on
824 seawater isotopic composition. *Earth Planet. Sci. Lett.* **432**, 404-414.

825 Berner R. A., Lasaga A. C. and Garrels R. M. (1983) The carbonate-silicate geochemical
826 cycle and its effect on atmospheric carbon-dioxide over the past 100 million years.
827 *Am. J. Sci.* **283**, 641-683.

828 Bouchez J., von Blanckenburg F. and Schuessler J. A. (2013) Modeling novel stable
829 isotope ratios in the weathering zone. *Am. J. Sci.* **313**, 267-308.

830 Bottomley D. J., Katz A., Chan L. H., Starinsky A., Douglas M., Clark I. D. and Raven K. G.
831 (1999) The origin and evolution of Canadian Shield brines: evaporation or freezing
832 of seawater? New lithium isotope and geochemical evidence from the Slave craton.
833 *Chem. Geol.* **155**, 295-320.

834 Calmels D., Galy A., Hovius N., Bickle M. J., West A. J., Chen M.-C. and Chapman H.
835 (2011) Contribution of deep groundwater to the weathering budget in a rapidly
836 eroding mountain belt, Taiwan. *Earth Planet. Sci. Lett.* **303**, 48-58.

837 Chan L. H., Edmond J. M., Thompson G. and Gillis K. (1992) Lithium isotopic composition
838 of submarine basalts - Implications for the lithium cycle in the oceans. *Earth Planet.*
839 *Sci. Lett.* **108**, 151-160.

840 Chen J., He D. and Cui S. (2003) The response of river water quality and quantity to the

841 development of irrigated agriculture in the last 4 decades in the Yellow River basin,
842 China. *Water Resour. Res.* **39**, 3, 1047, doi:10.1029/2001WR001234.

843 Chen J., Ke D., Zhao X., Fukushima Y. and Taniguchi M. (2006) Characteristics of
844 sediment and nutrient flows in the lower reach of the Yellow River. *Iahs-Aish P* **308**,
845 612-616.

846 Chen J., Wang F., Meybeck M., He D., Xia X. and Zhang L. (2005) Spatial and temporal
847 analysis of water chemistry records (1958-2000) in the Huanghe (Yellow River)
848 basin. *Global Biogeochem. Cycle* **19**, GB3016, doi:10.1029/2004GB002325.

849 Chetelat B., Liu C. Q., Zhao Z. Q., Wang Q. L., Li S. L., Li J. and Wang B. L. (2008)
850 Geochemistry of the dissolved load of the Changjiang Basin rivers: Anthropogenic
851 impacts and chemical weathering. *Geochim. Cosmochim. Acta* **72**, 4254-4277.

852 Clergue C., Dellinger M., Buss H. L., Gaillardet J., Benedetti M. F. and Dessert C. (2015)
853 Influence of atmospheric deposits and secondary minerals on Li isotopes budget in
854 a highly weathered catchment, Guadeloupe (Lesser Antilles). *Chem. Geol.* **414**,
855 28-41.

856 Clift P. D., Hodges K. V., Heslop D., Hannigan R., Van Long H. and Calves G. (2008)
857 Correlation of Himalayan exhumation rates and Asian monsoon intensity. *Nat.*
858 *Geosci.* **1**, 875-880.

859 Coogan L. A., Gillis K. M., Pope M. and Spence J. (2017) The role of low-temperature
860 (off-axis) alteration of the oceanic crust in the global Li-cycle: Insights from the
861 Troodos ophiolite. *Geochim. Cosmochim. Acta* **203**, 201-215.

862 Damsté J. S. S., van Bentum E. C., Reichart G. J., Pross J. and Schouten S. (2010) A CO₂

863 decrease-driven cooling and increased latitudinal temperature gradient during the
864 mid-Cretaceous Oceanic Anoxic Event 2. *Earth Planet. Sci. Lett.* **293**, 97-103.

865 Dellinger M., Bouchez J., Gaillardet J., Faure L. and Moureau J. (2017) Tracing
866 weathering regimes using the lithium isotope composition of detrital sediments.
867 *Geology* **45**, 411-414.

868 Dellinger M., Gaillardet J., Bouchez J., Calmels D., Galy V., Hilton R. G., Louvat P. and
869 France-Lanord C. (2014) Lithium isotopes in large rivers reveal the cannibalistic
870 nature of modern continental weathering and erosion. *Earth Planet. Sci. Lett.* **401**,
871 359-372.

872 Dellinger M., Gaillardet J., Bouchez J., Calmels D., Louvat P., Dosseto A., Gorge C.,
873 Alanoca L. and Maurice L. (2015) Riverine Li isotope fractionation in the Amazon
874 River basin controlled by the weathering regimes. *Geochim. Cosmochim. Acta* **164**,
875 71-93.

876 Fan B., Zhao Z. Q., Tao F., Li X., Tao Z., Gao S. and He M. (2016) The geochemical
877 behavior of Mg isotopes in the Huanghe basin, China. *Chem. Geol.* **426**, 19-27.

878 Faure G. and Mensing T. M. (2005) *Isotopes: Principles and Applications* (third edition).
879 John Wiley & Sons, New Jersey, 859-863.

880 Flesch G. D., Anderson Jr. A. R. and Svec H. J. (1973) A secondary isotopic standard for
881 $^6\text{Li}/^7\text{Li}$ determinations. *Int. J. Mass Spectrom. Ion Phys.* **12**, 265-272.

882 Forster A., Schouten S., Moriya K., Wilson P. A. and Damsté J. S. S. (2007) Tropical
883 warming and intermittent cooling during the Cenomanian/Turonian oceanic anoxic
884 event 2: Sea surface temperature records from the equatorial Atlantic.

885 *Paleoceanogr.* **22**, PA1219, doi:10.1029/2006PA001349.

886 Edmond J. M. (1992) Himalayan tectonics, weathering processes, and the strontium
887 isotope record in marine limestones. *Science* **258**, 1594-1597.

888 Gaillardet J., Dupre B., Louvat P. and Allegre C. J. (1999) Global silicate weathering and
889 CO₂ consumption rates deduced from the chemistry of large rivers. *Chem. Geol.*
890 **159**, 3-30.

891 Gaillardet J., Viers J. and Dupré B. (2014) Trace elements in river waters. In: Holland H. D.
892 and Turekian K. K., Eds. *Treatise on Geochemistry* (Second Edition). Elsevier,
893 Oxford, pp. 195-235.

894 Galy A. and France-Lanord C. (1999) Weathering processes in the Ganges-Brahmaputra
895 basin and the riverine alkalinity budget. *Chem. Geol.* **159**, 31-60.

896 Galy A, France-Lanord C. and Derry L. A. (1999) The strontium isotopic budget of
897 Himalayan Rivers in Nepal and Bangladesh. *Geochim. Cosmochim. Acta* **63**,
898 1905-1925.

899 Godsey S. E., Kirchner J. W. and Clow D. W. (2009) Concentration-discharge
900 relationships reflect chemostatic characteristics of US catchments. *Hydrol. Process.*
901 **23**, 1844-1864.

902 Gou L. F., Jin Z. D., Deng L., Sun H., Yu H. M. and Zhang F. (2017) Efficient purification for
903 Li and high-precision and accurate determination of Li isotopic compositions by
904 MC-ICP-MS. *Geochimica* **46**, 528-537 (in Chinese with English abstract).

905 Gou L. F., Jin Z. D., Deng L., He M. Y. and Liu C. Y. (2018) Effects of different cone
906 combinations on accurate and precise determination of Li isotopic composition by

907 MC-ICP-MS. *Spectrochim. Acta B* **146**, 1-8.

908 Hathorne E. C. and James R. H. (2006) Temporal record of lithium in seawater: A tracer
909 for silicate weathering? *Earth Planet. Sci. Lett.* **246**, 393-406.

910 Hathorne E. C., James R. H. and Lampitt R. S. (2009) Environmental versus
911 biomineralization controls on the intratest variation in the trace element composition
912 of the planktonic foraminifera *G. inflata* and *G. scitula*. *Paleoceanogr.* **24**, doi:
913 10.1029/2009PA001742.

914 Henchiri S., Gaillardet J., Dellinger M., Bouchez J. and Spencer R. G. M. (2016) Riverine
915 dissolved lithium isotopic signatures in low-relief central Africa and their link to
916 weathering regimes. *Geophys. Res. Lett.* **43**, 4391-4399.

917 Huang K. F., You C. F., Liu Y. H., Wang R. M., Lin P. Y. and Chung C. H. (2010)
918 Low-memory, small sample size, accurate and high-precision determinations of
919 lithium isotopic ratios in natural materials by MC-ICP-MS. *J. Anal. Atom. Spectrom.*
920 **25**, 1019-1024.

921 Huh Y., Chan L. H. and Edmond J. M. (2001) Lithium isotopes as a probe of weathering
922 processes: Orinoco River. *Earth Planet. Sci. Lett.* **194**, 189-199.

923 Huh Y., Chan L. H., Zhang L. and Edmond J. M. (1998) Lithium and its isotopes in major
924 world rivers: Implications for weathering and the oceanic budget. *Geochim.*
925 *Cosmochim. Acta* **62**, 2039-2051.

926 James R. H. and Palmer M. R. (2000) The lithium isotope composition of international
927 rock standards. *Chem. Geol.* **166**, 319-326.

928 Jeffcoate A. B., Elliott T., Kasemann S. A., Ionov D., Cooper K. and Brooker R. (2007) Li

929 isotope fractionation in peridotites and mafic melts. *Geochim. Cosmochim. Acta* **71**,
930 202-218.

931 Jiao J. Y., Wang Z. J., Zhao G. J., Wang W. Z. and Mu X. M. (2014) Changes in sediment
932 discharge in a sediment-rich region of the Yellow River from 1955 to 2010:
933 Implications for further soil erosion control. *J. Arid Land* **6**, 540-549.

934 Jin Z. D., You C. -F., Yu J., Wu L., Zhang F. and Liu H. -C. (2011) Seasonal contributions of
935 catchment weathering and eolian dust to river water chemistry, northeastern Tibetan
936 Plateau: Chemical and Sr isotopic constraints. *J. Geophys. Res.* **116**, doi:10.1029/
937 2011JF002002.

938 Kısakürek B., James R. H. and Harris N. B. W. (2005) Li and $\delta^7\text{Li}$ in Himalayan rivers:
939 Proxies for silicate weathering? *Earth Planet. Sci. Lett.* **237**, 387-401.

940 Lechler M., Pogge von Strandmann P. A. E., Jenkyns H. C., Prosser G. and Parente M.
941 (2015) Lithium-isotope evidence for enhanced silicate weathering during OAE 1a
942 (Early Aptian Selli event). *Earth Planet. Sci. Lett.* **432**, 210-222.

943 Lee C. T. A. (2008) Quantifying the relative roles of weathering and igneous processes on
944 crustal recycling and the origin of continental crust. *Geochim. Cosmochim. Acta* **72**,
945 A523-A523.

946 Lei X.-J., Li F., Zhao X.-M. and Center S. C. (2016) Evaluation and analysis of extreme
947 continuous precipitation induced disaster of Yan'an city in 2013 July. *Torrential Rain*
948 *Disasters* **35**, 521-528 (in Chinese with English abstract).

949 Lemarchand E., Chabaux F., Vigier N., Millot R. and Pierret M. C. (2010) Lithium isotope
950 systematics in a forested granitic catchment (Strengbach, Vosges Mountains,

951 France). *Geochim. Cosmochim. Acta* **74**, 4612-4628.

952 Li G. and West A. J. (2014) Evolution of Cenozoic seawater lithium isotopes: Coupling of
953 global denudation regime and shifting seawater sinks. *Earth Planet. Sci. Lett.* **401**,
954 284-293.

955 Li S., Xia, X., Zhou B., Zhang S., Zhang L. and Mou X. (2018) Chemical balance of the
956 Yellow River source region, the northeastern Qinghai-Tibetan Plateau: Insights
957 about critical zone reactivity. *Appl. Geochem.* **90**, 1-12.

958 Li W., Beard B. L., Li C. and Johnson C. M. (2014) Magnesium isotope fractionation
959 between brucite [Mg(OH)₂] and Mg aqueous species: Implications for silicate
960 weathering and biogeochemical processes. *Earth Planet. Sci. Lett.* **394**, 82-93.

961 Li Y. H., Teraoka H., Yang T. S. and Chen J. S. (1984) The elemental composition of
962 suspended particles from the Yellow and Yangtze Rivers. *Geochim. Cosmochim.*
963 *Acta* **48**, 1561-1564.

964 Liu C. Q., Zhao Z. Q., Wang Q. and Gao B. (2011) Isotope compositions of dissolved
965 lithium in the rivers Jinshajiang, Lancangjiang, and Nujiang: Implications for
966 weathering in Qinghai-Tibet Plateau. *Appl. Geochem.* **26**, S357-S359.

967 Liu T. S. (1988) *Loess in China*. 2nd edition, China Ocean Press, Beijing, p. 224.

968 Liu X. M., Rudnick R. L., McDonough W. F. and Cummings M. L. (2013) Influence of
969 chemical weathering on the composition of the continental crust: Insights from Li
970 and Nd isotopes in bauxite profiles developed on Columbia River Basalts. *Geochim.*
971 *Cosmochim. Acta* **115**, 73-91.

972 Liu X. M., Wanner C., Rudnick R. L. and McDonough W. F. (2015) Processes controlling

973 $\delta^7\text{Li}$ in rivers illuminated by study of streams and groundwaters draining basalts.
974 *Earth Planet. Sci. Lett.* **409**, 212-224.

975 Liu X. M. and Rudnick R. L. (2011) Constraints on continental crustal mass loss via
976 chemical weathering using lithium and its isotopes. *Proc. Nat. Acad. Sci. USA* **108**,
977 20873-20880.

978 Magna T., Wiechert U. H. and Halliday A. N. (2004) Low-blank isotope ratio measurement
979 of small samples of lithium using multiple-collector ICPMS. *Int. J. Mass Spectrom.*
980 **239**, 67-76.

981 Maher K. (2011) The role of fluid residence time and topographic scales in determining
982 chemical fluxes from landscapes. *Earth Planet. Sci. Lett.* **312**, 48-58.

983 Marschall H. R., Pogge von Strandmann P. A. E., Seitz H. M., Elliott T. and Niu Y. L. (2007)
984 The lithium isotopic composition of orogenic eclogites and deep subducted slabs.
985 *Earth Planet. Sci. Lett.* **262**, 563-580.

986 Mavromatis V., Rinder T., Prokushkin A. S., Pokrovsky O. S., Korets M. A., Chmeleff J.
987 and Oelkers E. H. (2016) The effect of permafrost, vegetation, and lithology on Mg
988 and Si isotope composition of the Yenisey River and its tributaries at the end of the
989 spring flood. *Geochim. Cosmochim. Acta* **191**, 32-46.

990 Millot R., Petelet-Giraud E., Guerrot C. and Négrel P. (2010a) Multi-isotopic composition
991 ($\delta^7\text{Li}$ - $\delta^{11}\text{B}$ - δD - $\delta^{18}\text{O}$) of rainwaters in France: Origin and spatio-temporal
992 characterization. *Appl. Geochem.* **25**, 1510-1524.

993 Millot R., Scaillet B. and Sanjuan B. (2010b) Lithium isotopes in island arc geothermal
994 systems: Guadeloupe, Martinique (French West Indies) and experimental approach.

995 *Geochim. Cosmochim. Acta* **74**, 1852-1871.

996 Millot R., Vigier N. and Gaillardet J. (2010c) Behaviour of lithium and its isotopes during
997 weathering in the Mackenzie Basin, Canada. *Geochim. Cosmochim. Acta* **74**,
998 3897-3912.

999 Misra S. and Froelich P. N. (2012) Lithium isotope history of Cenozoic seawater: Changes
1000 in silicate weathering and reverse weathering. *Science* **335**, 818-823.

1001 Négrel P., Millot R., Brenot A. and Bertin C. (2010) Lithium isotopes as tracers of
1002 groundwater circulation in a peat land. *Chem. Geol.* **276**, 119-127.

1003 Pistiner J. S. and Henderson G. M. (2003) Lithium-isotope fractionation during continental
1004 weathering processes. *Earth Planet. Sci. Lett.* **214**, 327-339.

1005 Pogge von Strandmann P. A. E., Burton K. W., James R. H., van Calsteren P. and
1006 Gislason S. R. (2010) Assessing the role of climate on uranium and lithium isotope
1007 behaviour in rivers draining a basaltic terrain. *Chem. Geol.* **270**, 227-239.

1008 Pogge von Strandmann P. A. E., Burton K. W., James R. H., van Calsteren P., Gislason S.
1009 R. and Mokadem F. (2006) Riverine behaviour of uranium and lithium isotopes in an
1010 actively glaciated basaltic terrain. *Earth Planet. Sci. Lett.* **251**, 134-147.

1011 Pogge von Strandmann P. A. E., Burton K. W., Opfergelt S., Eiríksdóttir E. S., Murphy M.
1012 J., Einarsson A. and Gislason S. R. (2016) The effect of hydrothermal spring
1013 weathering processes and primary productivity on lithium isotopes: Lake Myvatn,
1014 Iceland. *Chem. Geol.* **445**, 4-13.

1015 Pogge von Strandmann P. A. E., Elliott T., Marschall H. R., Coath C., Lai Y. J., Jeffcoate A.
1016 B. and Ionov D. A. (2011) Variations of Li and Mg isotope ratios in bulk chondrites

1017 and mantle xenoliths. *Geochim. Cosmochim. Acta* **75**, 5247-5268.

1018 Pogge von Strandmann P. A. E., Frings P. J. and Murphy M. J. (2017) Lithium isotope
1019 behaviour during weathering in the Ganges Alluvial Plain. *Geochim. Cosmochim.*
1020 *Acta* **198**, 17-31.

1021 Pogge von Strandmann P. A. E., Burton K. W., James R. H., van Calsteren P., Gislason S.
1022 R. and Sigfusson B. (2008a) The influence of weathering processes on riverine
1023 magnesium isotopes in a basaltic terrain. *Earth Planet. Sci. Lett.* **276**, 187-197.

1024 Pogge von Strandmann P. A. E., James R. H., van Calsteren P., Gislason S. R. and
1025 Burton K. W. (2008b) Lithium, magnesium and uranium isotope behaviour in the
1026 estuarine environment of basaltic islands. *Earth Planet. Sci. Lett.* **274**, 462-471.

1027 Pogge von Strandmann P. A. E., Jenkyns H. C. and Woodfine R. G. (2013) Lithium
1028 isotope evidence for enhanced weathering during Oceanic Anoxic Event 2. *Nat.*
1029 *Geosci.* **6**, 668-672.

1030 Pogge von Strandmann P. A. E. and Henderson G. M. (2015) The Li isotope response to
1031 mountain uplift. *Geology* **43**, 67-70.

1032 Pogge von Strandmann P. A. E., Opfergelt S., Lai Y. J., Sigfusson B., Gislason S. R. and
1033 Burton K. W. (2012) Lithium, magnesium and silicon isotope behaviour
1034 accompanying weathering in a basaltic soil and pore water profile in Iceland. *Earth*
1035 *Planet. Sci. Lett.* **339**, 11-23.

1036 Qi H. P., Coplen T. B., Wang Q. Z. and Wang Y. H. (1997) Unnatural isotopic composition
1037 of lithium reagents. *Anal. Chem.* **69**, 4076-4078.

1038 Ran L. S., Lu X. X., Sun H. G., Han J. T. and Yu R. H. (2015) Chemical denudation in the

1039 Yellow River and its geomorphological implications. *Geomorphology* **231**, 83-93.

1040 Ravizza G. and Esser B. K. (1993) A possible link between the seawater osmium isotope
1041 record and weathering of ancient sedimentary organic-matter. *Chem. Geol.* **107**,
1042 255-258.

1043 Roy S., Gaillardet J. and Allegre C. J. (1999) Geochemistry of dissolved and suspended
1044 loads of the Seine river, France: Anthropogenic impact, carbonate and silicate
1045 weathering. *Geochim. Cosmochim. Acta* **63**, 1277-1292.

1046 Ryu J. S., Vigier N., Lee S. W., Lee K. S. and Chadwick O. A. (2014) Variation of lithium
1047 isotope geochemistry during basalt weathering and secondary mineral
1048 transformations in Hawaii. *Geochim. Cosmochim. Acta* **145**, 103-115.

1049 Saito Y., Yang Z. S. and Hori K. (2001) The Huanghe (Yellow River) and Changjiang
1050 (Yangtze River) deltas: a review on their characteristics, evolution and sediment
1051 discharge during the Holocene. *Geomorphology* **41**, 219-231.

1052 Sauzeat L., Rudnick R. L., Chauvel C., Garcon M. and Tang M. (2015) New perspectives
1053 on the Li isotopic composition of the upper continental crust and its weathering
1054 signature. *Earth Planet. Sci. Lett.* **428**, 181-192.

1055 Taylor S. R., McLennan S. M. and McCulloch M. T. (1983) Geochemistry of loess,
1056 continental crustal composition and crustal model ages. *Geochim. Cosmochim.*
1057 *Acta* **47**, 1897-1905.

1058 Teng F. Z., Li W. Y., Rudnick R. L. and Gardner L. R. (2010) Contrasting lithium and
1059 magnesium isotope fractionation during continental weathering. *Earth Planet. Sci.*
1060 *Lett.* **300**, 63-71.

1061 Teng F. Z., McDonough W. F., Rudnick R. L., Dalpé C., Tomascak P. B., Chappell B. W.
1062 and Gao S. (2004) Lithium isotopic composition and concentration of the upper
1063 continental crust. *Geochim. Cosmochim. Acta* **68**, 4167-4178.

1064 Tessier A., Campbell P. G. C. and Bisson M. (1979) Sequential extraction procedure for
1065 the speciation of particulate trace-metals. *Anal. Chem.* **51**, 844-851.

1066 Tipper E. T., Bickle M. J., Galy A., West A. J., Pomiès C. and Chapman H. J. (2006) The
1067 short term climatic sensitivity of carbonate and silicate weathering fluxes: Insight
1068 from seasonal variations in river chemistry. *Geochim. Cosmochim. Acta* **70**,
1069 2737-2754.

1070 Tipper E. T., Calmels D., Gaillardet J., Louvat P., Capmas F. and Dubacq B. (2012)
1071 Positive correlation between Li and Mg isotope ratios in the river waters of the
1072 Mackenzie Basin challenges the interpretation of apparent isotopic fractionation
1073 during weathering. *Earth Planet. Sci. Lett.* **333-334**, 35-45.

1074 Tsai P. H., You C. F., Huang K. F., Chung C. H. and Sun Y. B. (2014) Lithium distribution
1075 and isotopic fractionation during chemical weathering and soil formation in a loess
1076 profile. *J. Asian Earth Sci.* **87**, 1-10.

1077 van Hoecke K., Belza J., Croymans T., Misra S., Claeys P. and Vanhaecke F. (2015)
1078 Single-step chromatographic isolation of lithium from whole-rock carbonate and clay
1079 for isotopic analysis with multi-collector ICP-mass spectrometry. *J. Anal. Atom.*
1080 *Spectrom.* **30**, 2533-2540.

1081 Verney-Carron A., Vigier N. and Millot R. (2011) Experimental determination of the role of
1082 diffusion on Li isotope fractionation during basaltic glass weathering. *Geochim.*

1083 *Cosmochim. Acta* **75**, 3452-3468.

1084 Vigier N., Decarreau A., Millot R., Carignan J., Petit S. and France-Lanord C. (2008)
1085 Quantifying Li isotope fractionation during smectite formation and implications for
1086 the Li cycle. *Geochim. Cosmochim. Acta* **72**, 780-792.

1087 Vigier N., Gislason S. R., Burton K. W., Millot R. and Mokadem F. (2009) The relationship
1088 between riverine lithium isotope composition and silicate weathering rates in
1089 Iceland. *Earth Planet. Sci. Lett.* **287**, 434-441.

1090 Vigier N. and Godd ris Y. (2015) A new approach for modeling Cenozoic oceanic lithium
1091 isotope paleo-variations: The key role of climate. *Clim. Past* **11**, 635-645.

1092 Walker J. C. G., Hays P. B. and Kasting J. F. (1981) A negative feedback mechanism for
1093 the long-term stabilization of Earth's surface temperature. *J. Geophys. Res.-Oceans*
1094 **86**, 9776-9782.

1095 Wang H., Bi N., Saito Y., Wang Y., Sun X., Zhang J. and Yang Z. (2010) Recent changes
1096 in sediment delivery by the Huanghe (Yellow River) to the sea: Causes and
1097 environmental implications in its estuary. *J. Hydrol.* **391**, 302-313.

1098 Wang H., Yang Z., Saito Y., Liu J. P., Sun X. and Wang Y. (2007) Stepwise decreases of
1099 the Huanghe (Yellow River) sediment load (1950–2005): Impacts of climate change
1100 and human activities. *Global Planet. Change* **57**, 331-354.

1101 Wang Q. L., Chetelat B., Zhao Z. Q., Ding H., Li S. L., Wang B.L., Li J. and Liu X. L. (2015)
1102 Behavior of lithium isotopes in the Changjiang River system: Sources effects and
1103 response to weathering and erosion. *Geochim. Cosmochim. Acta* **151**, 117-132.

1104 Wanner C., Sonnenthal E. L. and Liu X. M. (2014) Seawater $\delta^7\text{Li}$: A direct proxy for global

1105 CO₂ consumption by continental silicate weathering? *Chem. Geol.* **381**, 154-167.

1106 West A. J., Galy A. and Bickle M. (2005) Tectonic and climatic controls on silicate
1107 weathering. *Earth Planet. Sci. Lett.* **235**, 211-228.

1108 Wimpenny J., Colla C. A., Yu P., Yin Q. Z., Rustad J. R. and Casey W. H. (2015) Lithium
1109 isotope fractionation during uptake by gibbsite. *Geochim. Cosmochim. Acta* **168**,
1110 133-150.

1111 Wimpenny J., Gislason S. R., James R. H., Gannoun A., Pogge von Strandmann P. A. E.
1112 and Burton K. W. (2010) The behaviour of Li and Mg isotopes during primary phase
1113 dissolution and secondary mineral formation in basalt. *Geochim. Cosmochim. Acta*
1114 **74**, 5259-5279.

1115 Wu L., Huh Y., Qin J., Du G. and van Der Lee S. (2005) Chemical weathering in the Upper
1116 Huang He (Yellow River) draining the eastern Qinghai-Tibet Plateau. *Geochim.*
1117 *Cosmochim. Acta* **69**, 5279-5294.

1118 Wu W., Xu S., Yang J. and Yin H. (2008) Silicate weathering and CO₂ consumption
1119 deduced from the seven Chinese rivers originating in the Qinghai-Tibet Plateau.
1120 *Chem. Geol.* **249**, 307-320.

1121 Yokoo Y., Nakano T., Nishikawa M. and Quan H. (2004) Mineralogical variation of Sr–Nd
1122 isotopic and elemental compositions in loess and desert sand from the central
1123 Loess Plateau in China as a provenance tracer of wet and dry deposition in the
1124 northwestern Pacific. *Chem. Geol.* **204**, 45-62.

1125 Yu Y., Wang H., Shi X., Ran X., Cui T., Qiao S. and Liu Y. (2013) New discharge regime of
1126 the Huanghe (Yellow River): Causes and implications. *Cont. Shelf Res.* **69**, 62-72.

- 1127 Zachos J., Pagani M., Sloan L., Thomas E. and Billups K. (2001) Trends, rhythms, and
1128 aberrations in global climate 65 Ma to present. *Science* **292**, 686-693.
- 1129 Zhang J., Huang W. W., Letolle R. and Jusserand C. (1995) Major element chemistry of
1130 the Huanghe (Yellow River), China - weathering processes and chemical fluxes. *J.*
1131 *Hydrol.* **168**, 173-203.
- 1132 Zhang J., Huang W. W. and Shi M. C. (1990) Huanghe (Yellow-River) and its estuary -
1133 Sediment origin, transport and deposition. *J. Hydrol.* **120**, 203-223.
- 1134 Zhang Q., Jin Z., Zhang F. and Xiao J. (2015) Seasonal variation in river water chemistry
1135 of the middle reaches of the Yellow River and its controlling factors. *J. Geochem.*
1136 *Explor.* **156**, 101-113.
- 1137 Zhao G. J., Tian P., Mu X. M., Jiao J. Y., Wang F. and Gao P. (2014) Quantifying the
1138 impact of climate variability and human activities on streamflow in the middle
1139 reaches of the Yellow River basin, China. *J. Hydrol.* **519**, 387-398.
- 1140

Table 1 Li concentrations and Li isotopic ratios of dissolved load and suspended particulate matter (SPM) of river waters collected weekly from the middle Yellow River.

See [Zhang et al. \(2015\)](#) for major cation concentrations.

Sample no.	Date of 2013 (dd-mm)	Water discharge ^a m ³ /s	T ^{a, b} (°C)	pH ^a	TDS ^{a, c} (mg/L)	River water			SPM		
						Li	δ ⁷ Li	2 s.d. ^d	Li	δ ⁷ Li	2 s.d. ^d
						umol/L	‰	‰	μg/g	‰	‰
LM13-1	5-Jan	588.3	0.0	7.64	1063	3.95	18.9	0.1	37.6	2.3	0.3
LM13-2	12-Jan	456.4	1.1	7.88	1066	4.15	18.3	0.3			
LM13-3	19-Jan	468.0	0.1	7.93	905	3.34	19.4	0.2			
LM13-4	26-Jan	474.8	1.4	7.89	913	3.29	20.1	0.0	30.9	2.9	0.1
LM13-5	2-Feb	527.7	1.1	8.06	831	3.02	19.3	0.3	55.5	3.5	0.0
LM13-6	9-Feb	518.8	0.6	8.13	766	2.89	19.2	0.3			
LM13-7	16-Feb	609.1	2.0	8.05	735	2.68	18.9	0.4			
LM13-8	23-Feb	560.4	1.9	8.02	702	2.67	18.8	0.5			
LM13-9	2-Mar	832.0	5.0	7.87	671	2.50	18.9	0.1	39.4	2.5	0.0
LM13-10	10-Mar	854.5	5.3	7.73	654	2.41	19.1	0.2			
LM13-11	16-Mar	1110.1	7.1	7.89	629	2.41	18.8	0.3			
LM13-12	23-Mar	1513.6	7.9	7.93	600	2.22	20.5	0.4			
LM13-13	30-Mar	402.9	12.5	7.86	768	2.84	19.8	0.2			
LM13-14	6-Apr	845.9	10.7	7.86	806	2.88	19.4	0.1	51.6	1.0	0.3
LM13-15	13-Apr	647.8	15.1	8.01	656	2.59	18.5	0.2			
LM13-16	20-Apr	680.1	11.4	8.01	607	2.42	19.2	0.3			
LM13-17	27-Apr	338.3	14.5	8.07	627	2.69	19.4	0.3			
LM13-18	4-May	284.1	15.6	7.94	612	2.79	19.1	0.1	37.7	1.9	0.5
LM13-19	11-May	318.7	16.3	8.13	627	2.84	19.0	0.2			
LM13-20	18-May	167.3	15.0	7.83	635	3.56	18.4	0.4			
LM13-21	25-May	179.2	16.4	7.78	633	2.49	17.5	0.6			
LM13-22	1-Jun	225.0	18.6	7.82	614	2.92	17.3	0.3			
LM13-23	8-Jun	971.8	23.8	7.80	590	2.50	16.9	0.3			
LM13-24	15-Jun	687.1	23.7	7.86	620	2.41	17.3	0.8			
LM13-25	22-Jun	773.6	22.7	7.83	576	2.51	17.0	0.5			
LM13-26	29-Jun	493.2	20.1	7.55	573	2.36	17.0	0.4	48.9	0.6	0.4
LM13-27	2-Jul	1276.3	27.7	7.99	553	2.73	17.9	0.2			
LM13-28	8-Jul	589.6	27.7	7.83	587	2.84	17.4	0.5			
LM13-29	12-Jul	1353.8	24.2	7.73	617	2.98	18.4	0.5			
LM13-30	18-Jul	1350.9	25.0	7.83	599	2.91	18.2	0.4			
LM13-31	22-Jul	2400.5	23.3	7.66	542	2.57	18.8	0.4			
LM13-32	23-Jul	2207.6	22.3	8.14	527	2.72	18.5	0.2			
LM13-33	24-Jul	1452.5	26.1	7.05	598	2.63	18.7	0.2	32.6	2.2	0.3
LM13-34	25-Jul	2255.6	25.4	7.22	603	3.23	20.0	0.2			

LM13-35	31-Jul	990.3	25.6	7.71	671	2.90	18.8	0.1			
LM13-36	7-Aug	1370.0	24.5	8.02	623	2.78	18.4	0.4			
LM13-37	12-Aug	1634.2	26.2	7.92	671	2.94	18.8	0.1			
LM13-38	18-Aug	1106.8	28.8	7.89	658	2.78	18.5	0.3			
LM13-39	23-Aug	1093.3	25.6	7.85	665	2.69	17.9	0.1			
LM13-40	30-Aug	1205.7	23.6	8.30	621	2.70	18.6	0.3	28.9	2.1	0.2
LM13-41	4-Sep	1392.3	23.2	8.30	622	2.69	18.1	0.1			
LM13-42	10-Sep	1238.6	21.7	8.31	616	2.63	18.5	0.2			
LM13-43	11-Sep	1745.0	21.1	8.30	626	2.61	18.9	0.3			
LM13-44	16-Sep	1715.6	22.0	8.30	583	2.57	18.6	0.1	31.2	1.8	0.4
LM13-45	18-Sep	1213.0	21.4	8.23	558	2.53	18.4	0.2			
LM13-46	19-Sep	1723.3	21.1	7.87	548	2.26	18.9	0.3			
LM13-47	26-Sep	1211.0	17.6	8.71	585	2.41	19.8	0.2			
LM13-48	2-Oct	901.3	19.3	8.48	652	2.53	19.4	0.2	43.4	0.6	0.3
LM13-49	9-Oct	797.3	20.2	8.28	693	2.66	20.1	0.1			
LM13-50	16-Oct	789.6	15.3	8.40	649	2.49	18.9	0.3			
LM13-51	23-Oct	310.9	11.7	8.32	577	2.32	20.1	0.1			
LM13-52	30-Oct	604.7	11.6	7.72	611	2.44	19.7	0.1			
LM13-53	6-Nov	312.2	12.3	8.08	647	3.02	19.0	0.1			
LM13-54	13-Nov	219.8	8.6	8.23	709	3.20	20.1	0.2			
LM13-55	20-Nov	205.4	5.6	7.32	701	3.01	18.6	0.1			
LM13-56	27-Nov	573.4	4.3	7.51	741	2.78	20.6	0.3	36.7	0.8	0.1
LM13-57	4-Dec	1113.9	3.0	7.70	697	2.54	21.0	0.3			
LM13-58	11-Dec	712.1	1.7	7.92	807	4.41	17.5	0.1			
LM13-59	18-Dec	626.7	0.8	7.89	847	3.06	21.5	0.1			
LM13-60	25-Dec	398.7	0.3	8.30	873	3.13	21.2	0.2	68.9	1.8	0.1

a Data from Zhang et al. (2015);

b T, water temperature;

c TDS, total dissolved solids;

d 2 s.d., 2 times standard derivation.

Table 2 Concentrations of ions and anions of rain water samples collected at the Longmen hydrological station.

Sample no.	Date 2013 (mm-dd)	Na	Ca	Mg	K	Cl	SO ₄	NO ₃	F	Li
		(μmol/L)								
LM-r1	July-8	244	136	60	27	180	202	323	0.38	0.10
LM-r2	Aug-11	134	182	55	45	93	230	225	0.60	0.16
LM-r3	Aug-28	78	171	20	17	49	201	78	0.51	0.12

Major ionic concentrations are from [Zhang et al. \(2015\)](#).

Table 3 Li and Na concentrations and Li isotopic compositions of the evaporite fraction in

Lingtai loess profile.

Stratum	Na μmol/g	Li nmol/g	$\delta^7\text{Li}$ ‰	2 s.d. ‰
L1	20.9	1.5	23.0	0.3
S1	10.5	2.0	23.6	0.1
S5	42.3	1.7	21.0	0.1
L9	7.8	1.8	26.8	0.1
RC	3.5	1.3	/	/

2 s.d., 2 times standard deviation from triple analyses of the same solution.

Table 4 Li and Na concentrations and lithium isotopes compositions of the river bottom sand

(RBS) and sewage samples collected at the Longmen hydrological station.

Samples	Na	Li	$\delta^7\text{Li}$	2 s.d.
River bed sand (RBS)	658 $\mu\text{mol/g}$	5.3 $\mu\text{mol/g}$	6.9‰	0.1
Sewage (TKT1)	902 $\mu\text{mol/mL}$	12.3 $\mu\text{mol/L}$	23.8‰	0.2

2 s.d., 2 times standard deviation from triple analyses of the same solution.

Figure captions:

Figure 1. Sketch map of the Yellow River drainage basin, with major tributaries and sampling site (Longmen hydrological station). Lithologically, loess and desert dominate within the upper and middle reaches of the Yellow River basin. Inset map shows the Yellow River drainage basin.

Figure 2 (A) Li flux, (B) concentration of Li, and (C) $\delta^7\text{Li}$ of river waters collected weekly at the Longmen hydrological station over the whole year of 2013, and (D) $\delta^7\text{Li}$ of monthly suspended particulate matter (SPM). (G) SPM flux, (H) concentration of SPM and (I) physical erosion rate (PER, from [Zhang et al., 2015](#)) at the Longmen hydrological station over 2013, and (J) Li concentration of monthly SPM. All showing obvious seasonal variations, along with (E, K) water and air temperatures and (F, L) water discharge in both A and B panels. The intervals of ice melting (from 16th March to 13th April), monsoon season (from June to mid-September), and a storm event (22nd to 25th of July) were shaded by green, blue, and dark blue, respectively. The significant seasonal variation in Li and $\delta^7\text{Li}_{\text{rw}}$ ratios of dissolved load is observed with highest ratios in winter (dry seasons), whereas the Li concentrations ($42.4 \pm 11.6 \mu\text{g/g}$) and $\delta^7\text{Li}$ values ($1.85 \pm 0.89\text{‰}$) of SPM remains little variation over the year.

Figure 3 The suspended particulate matter (SPM) concentrations of the Toudaoguai (TDG) and Longmen (LM) hydrological stations (locations marked in Fig. 1) over 2013, showing that SPM was mainly derived from

loess between TDG and LM during the monsoon season.

Figure 4 Linear positive correlations of Li concentrations with (A) B, (B) Cl, (C) Na, and (D) SO₄, indicating significant contribution of evaporites from loess to Li in the river waters of the middle reaches of the Yellow River.

Figure 5 Mixing diagram of Li and $\delta^7\text{Li}$ of the Yellow River waters, indicating that Li and its isotopic ratios are controlled by seasonal processes and sources. Groundwater extrusion may prevail during the early monsoon when rains have been penetrating. Decreased $\delta^7\text{Li}$ but increased Li concentrations may be due to a SPM re-dissolution during the pre-monsoon. During the post monsoon, that evaporite dissolution triggered by a storm event contributed a bit more to river waters than other seasons. A sample (LM13-58) collected on 11th of December with abnormally high Li concentration and low isotopic ratio was excluded.

Figure 6 Partitioning of Li of the river water into five end-members, i.e. silicates, carbonates, anthropogenic, rain, and evaporites. In an annual average, silicates and evaporites contribute an average of ~60% and ~25% of the dissolved Li, respectively. It's notable that the evaporite contribution increased after the storm event.

Figure 7 Plot of Cl/Li against SO₄/Li, clearly showing the seasonal Li contribution variation sensitive to hydrological conditions. During the pre- and early monsoons, silicate contribution dominates, whereas evaporite contribution increases in the late monsoon, especially after the storm event.

Figure 8 (A) $\delta^7\text{Li}_{\text{rw}}$ of the Yellow River waters plotted against SPM concentrations, showing no overall trend of $\delta^7\text{Li}_{\text{rw}}$ values with SPM concentrations, indicating that Li isotopes in riverine system might be conservative. A sample collect on 11th of December with abnormally high Li concentration and low isotopic ratio was excluded. (B) A negative correlation of $1000 \cdot \alpha_{\text{water-clay}}$ (i.e. $\delta^7\text{Li}_{\text{rw}} - \delta^7\text{Li}_{\text{loess}}$, $\delta^7\text{Li}_{\text{loess}} = 0$, [Teng et al., 2004](#)) of the Yellow River waters against water temperature fitted using Isoplot®, the fitted A and B parameters in Eq. (6) are 1.82 ± 0.54 and -2.9 ± 6.5 , respectively, indicating a temperature dependent of $\delta^7\text{Li}_{\text{rw}}$ within the Yellow River basin. Note that the samples might affected by SPM re-dissolution (Fig. 5, $[\text{Li}] > 3.15$ in Table 2) were excluded. See text for details.

Figure 9 Power positive correlation between Li_{sil} flux (Li in river water derived from silicate dissolution) of dissolved load and physical erosion rate (PER, from [Zhang et al. \(2015\)](#)), further supporting that erosion rate is of great importance for chemical weathering as proposed by [Gaillardet et al. \(1999\)](#) and for Li isotopes by [Li and West \(2014\)](#), especially in such easy-erodible loess covered region.

Figure 10 Temperature dependent Li isotopic fractionation was fitted with $\delta^7\text{Li}_{\text{rw}} = 22\text{‰}$ at 20°C from [Li and West \(2014\)](#). Direct fitted values (blue points) are higher than the measured data systematically. Our best fit according to Eq. (6) and Fig. 8B is shown by the red points on the graph,

suggesting that temperature is the dominant player controlling the $\delta^7\text{Li}_{rw}$.

The averaged $\delta^7\text{Li}_{\text{loess}} = 0$ was set as the initial $\delta^7\text{Li}$ value for both fittings

([Teng et al., 2004](#)).

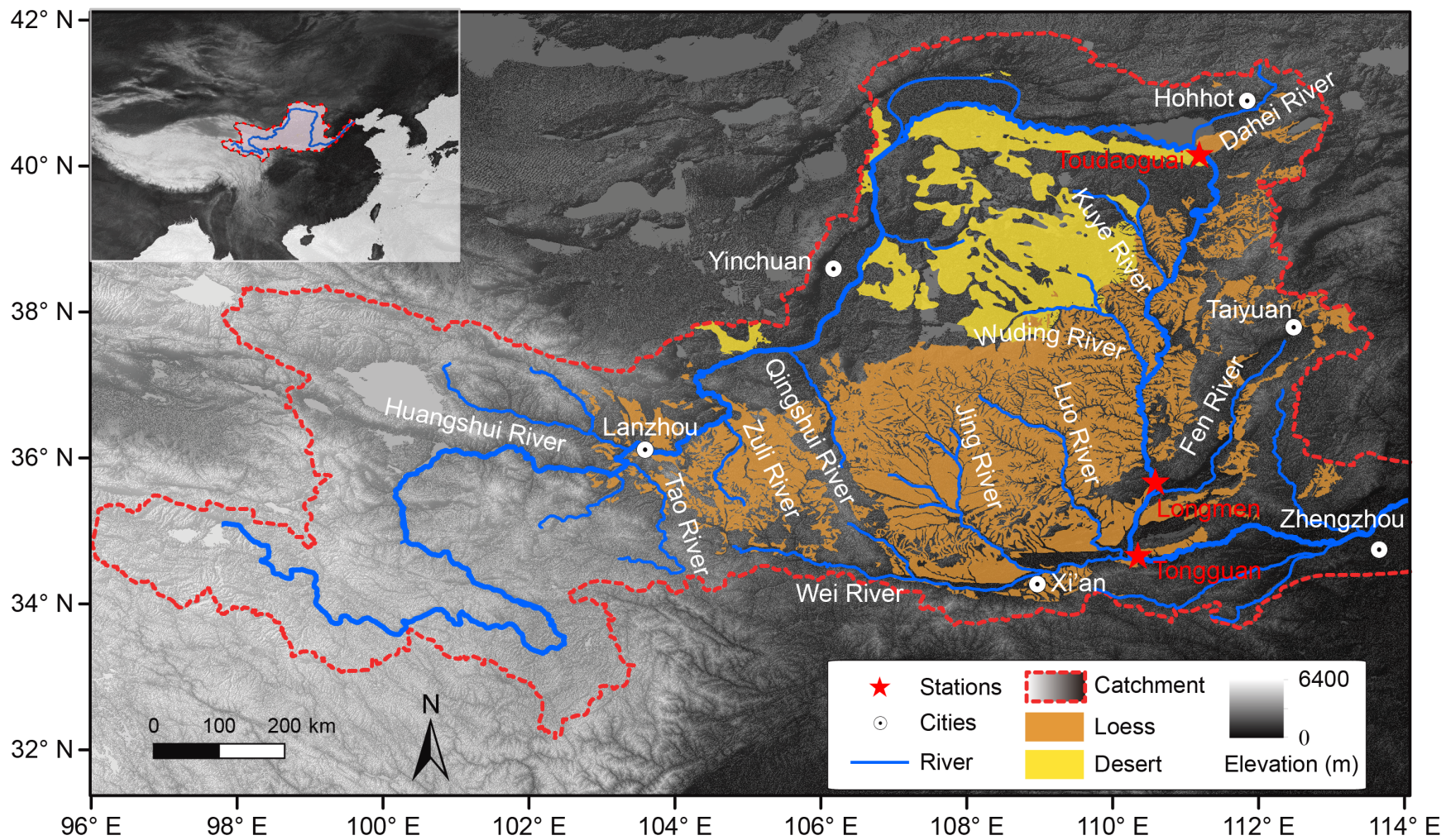


Figure 1

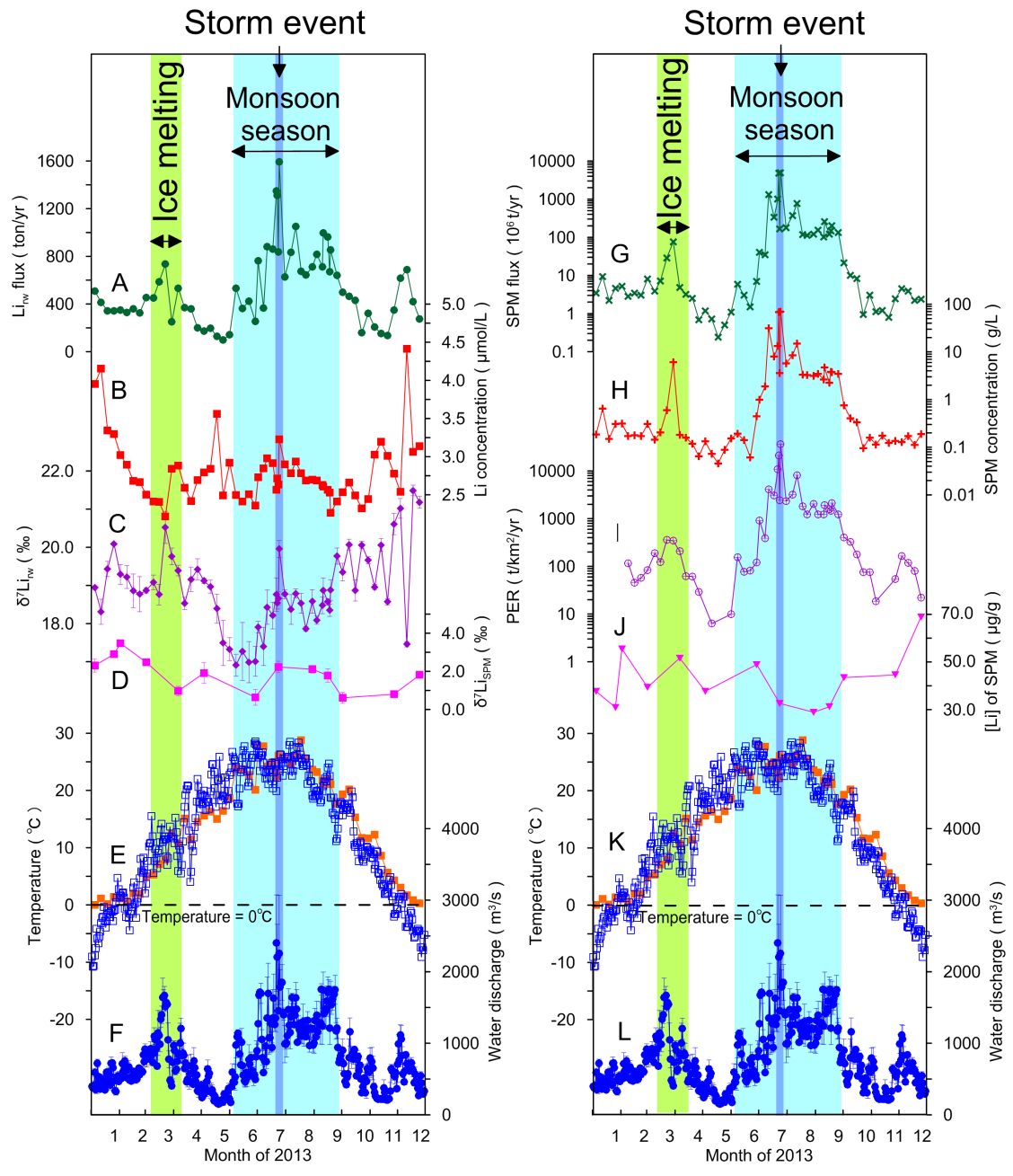
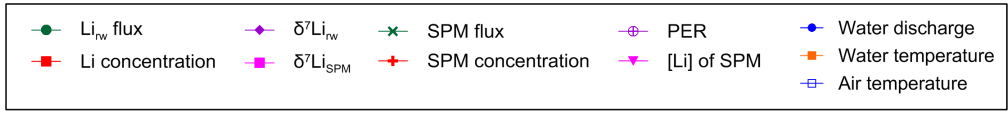


Figure 2

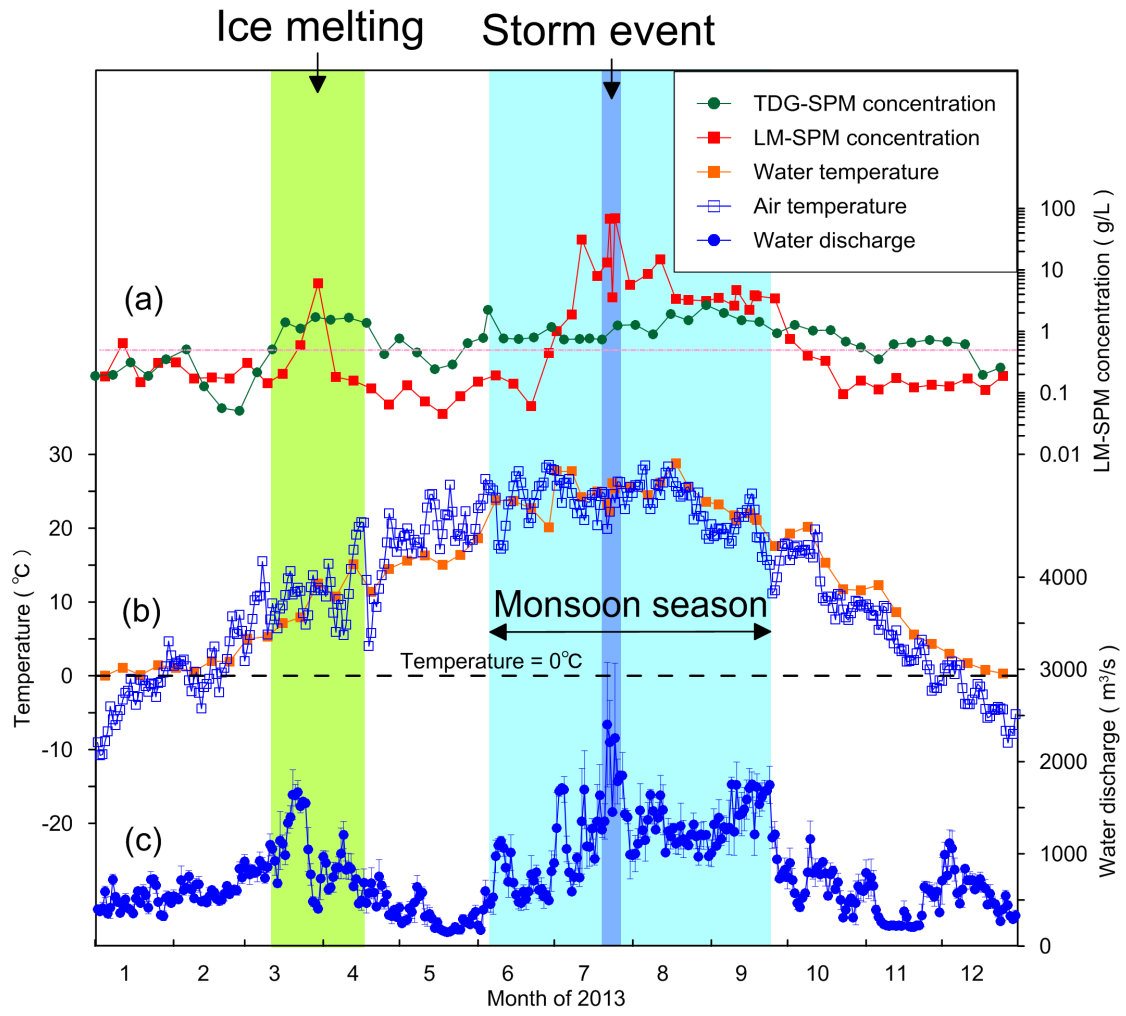


Figure 3

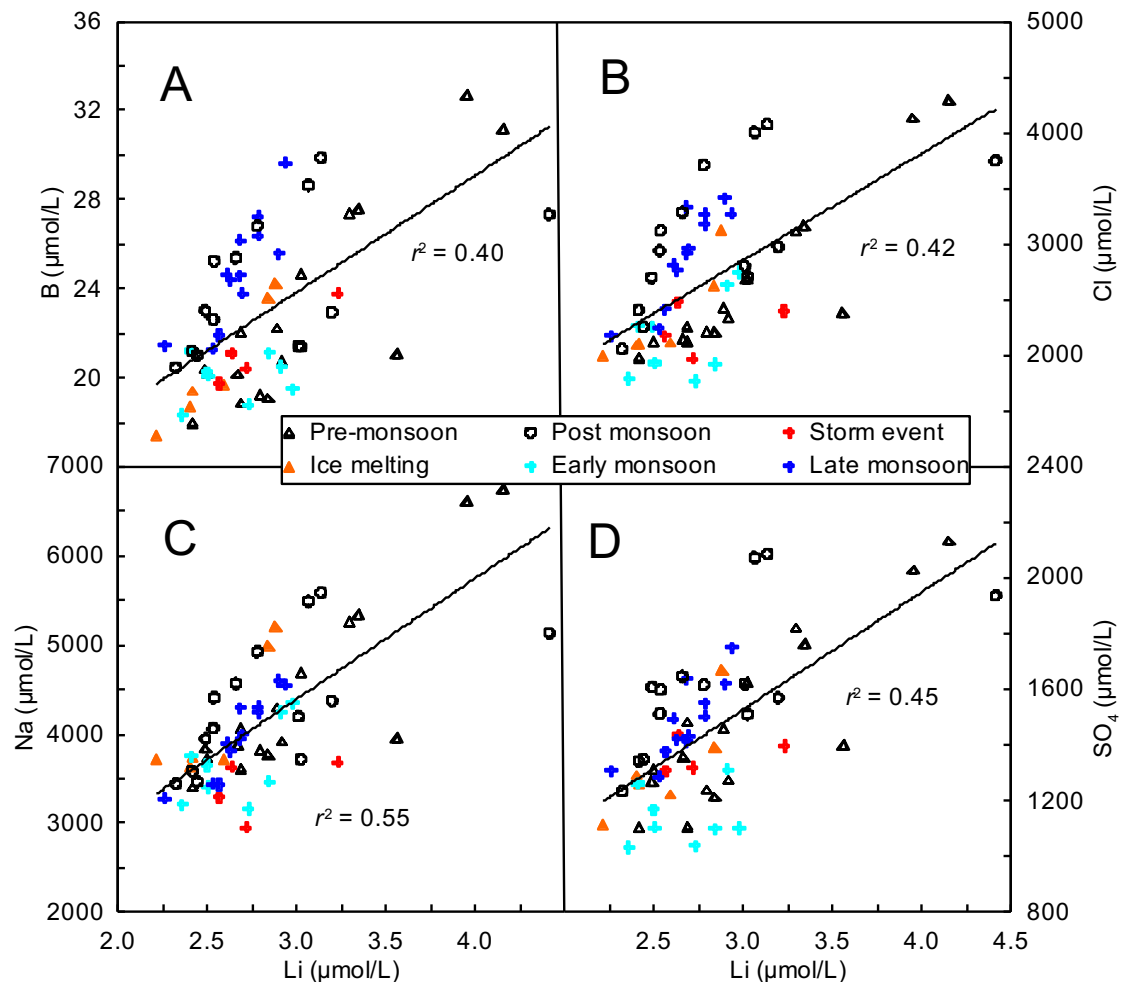


Figure 4

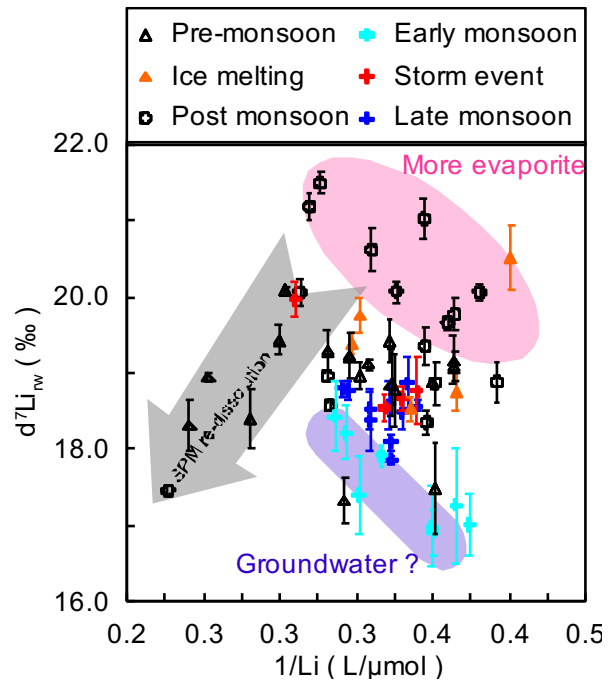


Figure 5

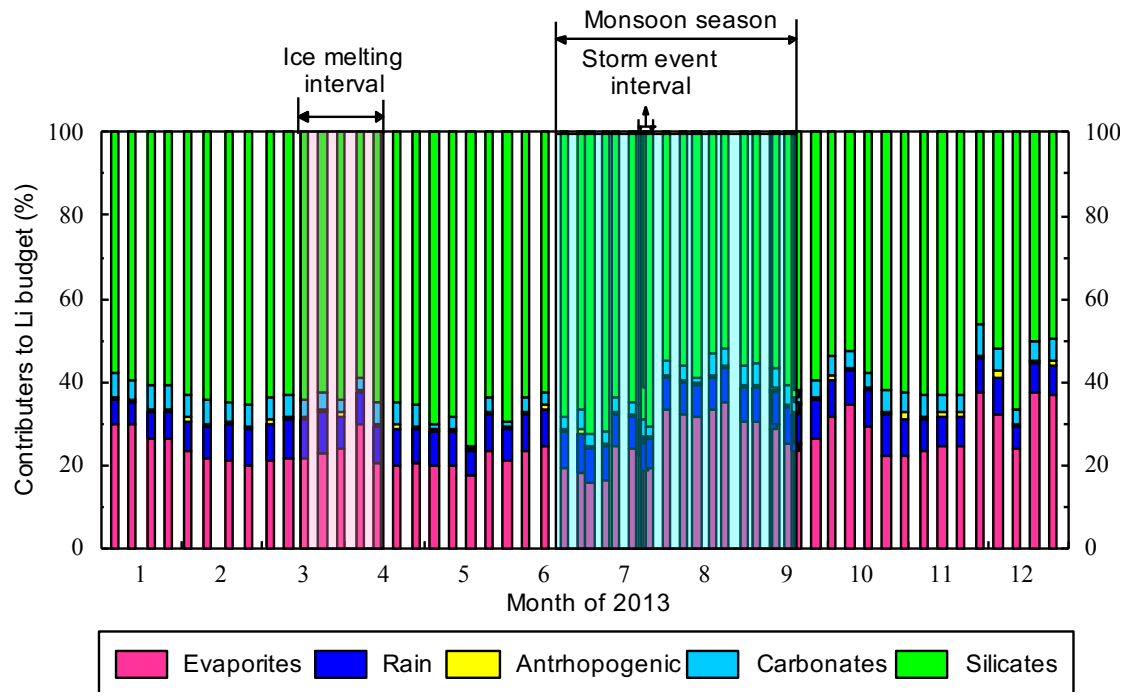


Figure 6

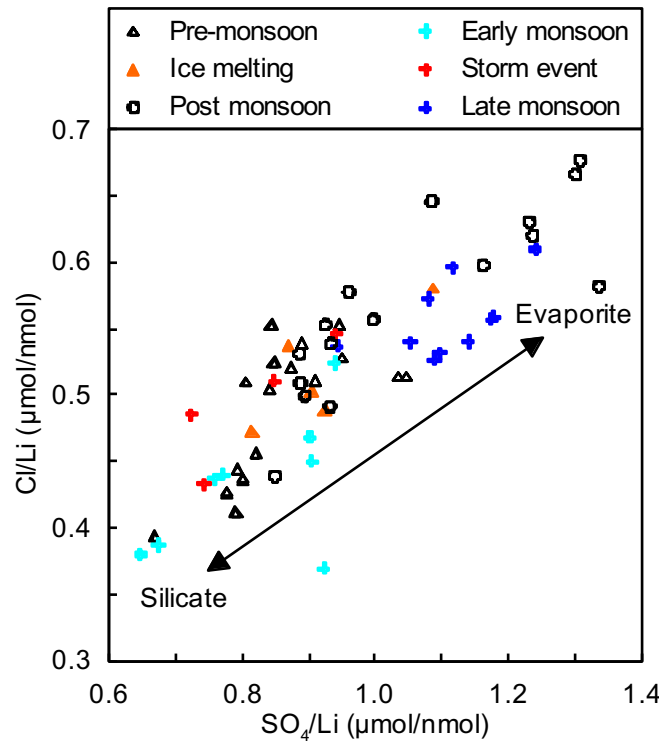


Figure 7

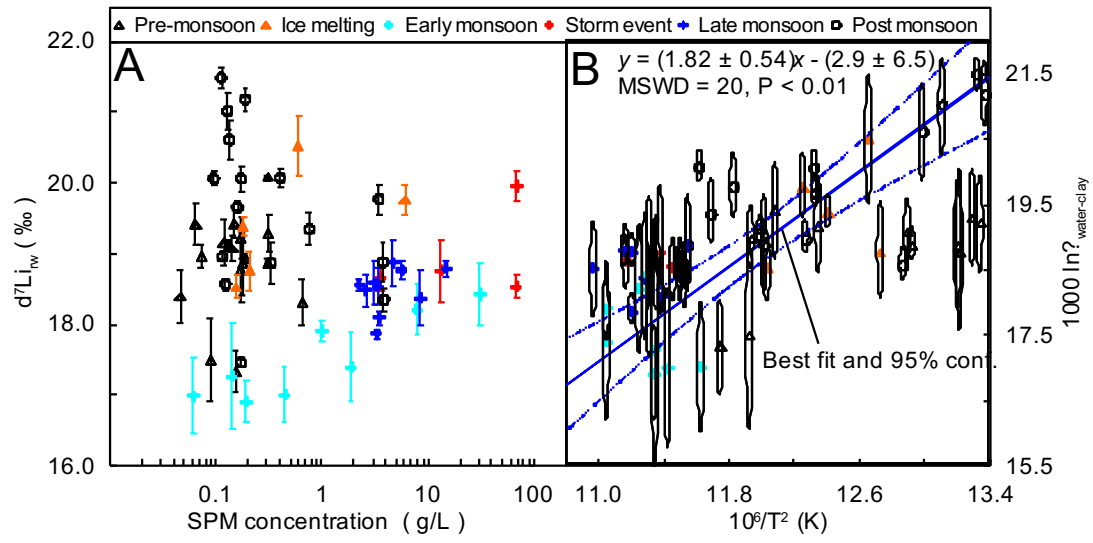


Figure 8

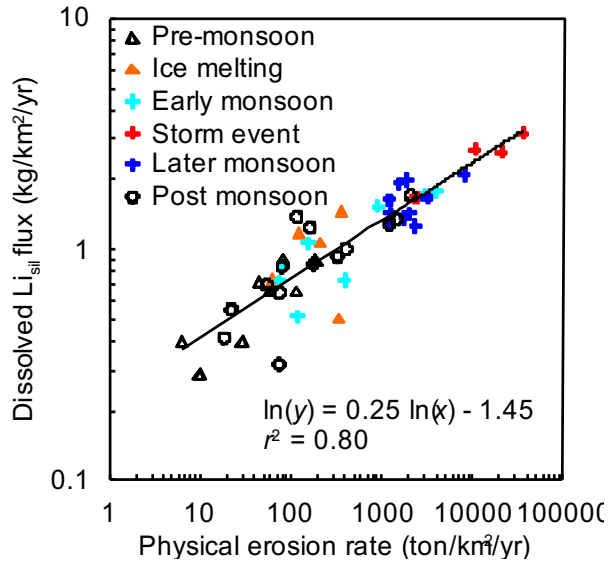


Figure 9

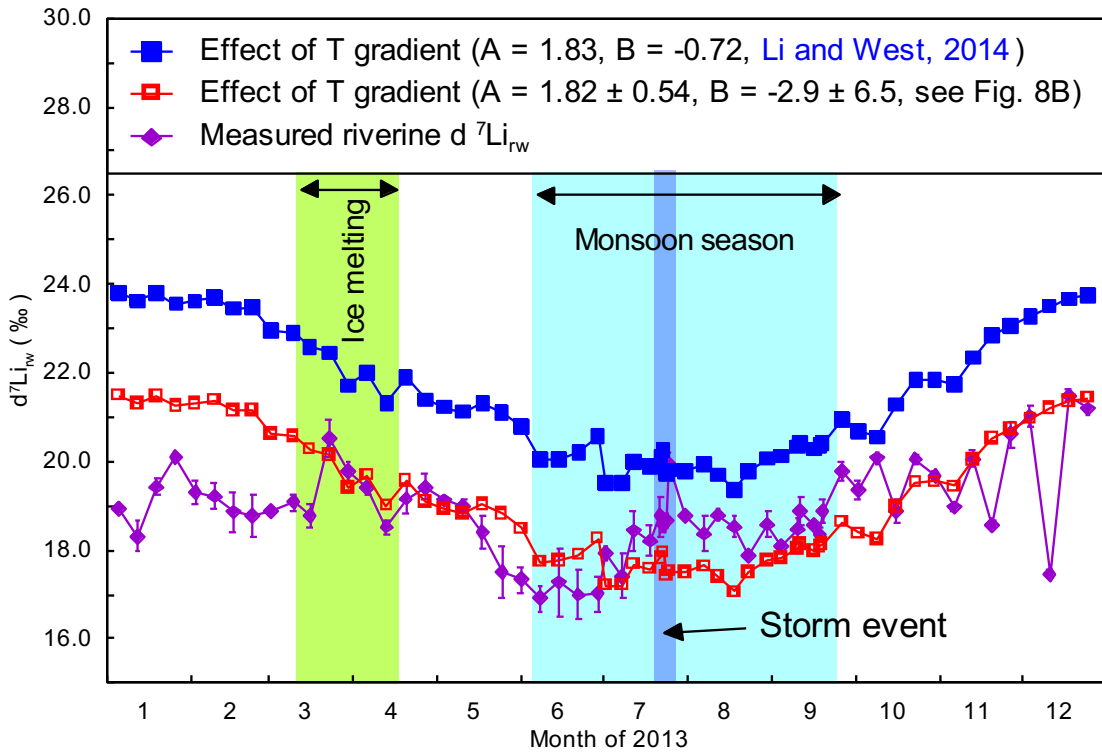


Figure 10